Diogo Rodrigues Francisco Sabino

Bachelor in Micro and Nanotechnologies Engineering

3D Printing of Nanoreinforced Pectin-Based Hydrogels with Tunable Flow Properties for Bone Regeneration

Dissertation submitted in partial fulfillment
of the requirements for the degree of

Master of Science in
Micro and Nanotechnologies Engineering

Adviser: Dr. Miguel Dias Castilho, Associate Professor,
Department of Orthopaedics, University Medical Centre Utrecht

Co-adviser: Dr. João Paulo Borges, Associate Professor, Faculty of Sciences and Technology, NOVA University of Lisbon

Examination committee:

Chair: Prof. Dr. Hugo Manuel Águas

Repporteurs: Profª. Dr. Célia Maria Henriques

Members: Prof. Dr. João Paulo Borges

FACULDADE DE CIÊNCIAS E TECNOLOGIA
UNIVERSIDADE NOVA DE LISBOA

October, 2019

3D Printing of Nanoreinforced Pectin-Based Hydrogels with Tunable Flow Properties for Bone Regeneration

"Once you stop learning, you start dying."

- Albert Einstein

Acknowledgements

Finalizing this thesis means the world to me, both on a personal and academic level. I would like to acknowledge the importance of all the people without whom this would not have been possible by thanking them with a few words.

Firstly, I would like to thank Professors Elvira Fortunato and Rodrigo Martins for have had the vision to institute Micro and Nanotechnology Engineering at NOVA University, an MSCs program that honors and prestige this university so well. CEMOP, DCM, and CENIMAT-i3N, our research hubs, are full of amazing and talented people that produce groundbreaking work in such amazing fields of study. I would also like to thank all of the joyful professors of this great department that taught me so much during these years, always encouraging us to work better and wisely. It was a real pleasure to be part of the first decade of all this and I wish you all the best.

To my supervisor Professor Dr. Miguel Castilho, for giving me a once in a lifetime opportunity to work in one of the worldwide top institutions in the field of biofabrication. I cannot express how thankful I am for it. Thanks for all the help and support during the 7 months I spent in The Netherlands, it was an honor working with you. It is also good to know that our country has such a great ambassador in Utrecht.

To Nasim, the best daily supervisor I could have ever asked for. Thanks for being so kind and generous to me, you made everything way easier. It was a pleasure working alongside you, and I'll definitely be praying for you until you finish your PhD.

To my co-supervisor Professor Dr. João Paulo Borges, for having accepted to be the guidance of my thesis in Portugal and for being the person that introduced me to the amazing field of biomaterials. If it wasn´t for your amazing classes, I would have not gone this way.

To all the people from the Department of Health Technology of Technical University of Denmark for the provided collaboration in this project, especially Mehdi Mehrali for all the time spent on helping us.

À minha família por todo o amor, amizade e apoio nos últimos 23 anos, começando pelos meus pais. Obrigado por todos os ensinamentos, por estarem sempre presentes e por acima de tudo serem meus amigos. Obrigado também pela peste que trouxeram ao mundo. Inês, obrigado por todo o apoio e por seres a melhor irmã do mundo. A ti avó, por teres sido tão importante durante toda a minha infância e adolescência, és como uma segunda mãe. Ao meu avô, por toda a ajuda prestada e por ter sempre uma história para contar. Às minhas tias Fatinha e Carla e respetivos tios Miguel e Alcindo, por todas as conversas e momentos passados em família. Às minhas primas, da mais crescida às 3 pirralhas que me moem o juízo. Aos que já partiram, um obrigado saudoso, guardem-me aí uma suite com uma vista daquelas.

A ti Leonor, que desde que entraste neste curso estiveste sempre a meu lado, sem hesitar. Faltam--me tantas palavras para ti. O mais sincero dos obrigados por tudo. Pelas gargalhadas, pelo apoio incondicional, pela cumplicidade. Pelo amor, pela paciência, pelas aventuras e pelas inúmeras lições que me abriram os olhos em tanta coisa, se cresci nestes 5 anos muito se deve a ti. Mesmo a mais de 2000 km de distância foste a minha maior ajuda e companhia, é assustador pensar como teria sido tudo isto sem ti. Grande parte disto também é e será sempre tua, espero que saibas isso. Aproveita os dois anos que te faltam por aqui, adoro-te.

Ao quarteto fantástico que me acompanhou do 1º ano até hoje: Rodrigo, Guilherme, Ricardo e Fred. Meus amigos, foi bonito e vai continuar a ser, mesmo que mais longe uns dos outros. Muitas histórias e momentos para recordar. Aos restantes manos do chat: Matos, Bernardo, Bártolo, Saraiva, Simão e Rodrigues. Obrigado por todos os memes, gargalhadas, conversas random e momentos de bullying, tornam os meus dias bastante mais interessantes e divertidos.

A todos os outros amigos e colegas de 14/15, que duma maneira ou doutra tiveram influência ao longo destes anos. Um ano para recordar na história deste curso, sem a mínima dúvida.

To all the people in University Medical Centre Utrecht and Hubtrecht Institute, especially the friends I made: João, Fady, Yiannis and Cody, what a pleasure it was to get to know you all, we really had a blast during these 7 months. John, Tessa, Devon, Marta, Bruno, Duilia and Bastiaan, a big thanks to you guys as well. I loved every second of it, couldn't have asked for better friends and lab mates. I just hope we can all meet again soon somewhere around the world. Preferably with a different outfit, enough with the gloves and the lab coat.

Aos meus amigos seixalenses. Santos, Martim, Capitulo, Gonçalo, Velez, Travanca, Inês e Marianas. Por todos os debates, da política ao futebol, e por todos estes anos de amizade.

A todos aqueles que não foram acima mencionados, mas que deixaram a sua marca neste trajeto, o meu muito obrigado.

Resumo

Os hidrogéis têm demonstrado ser alternativas altamente atrativas para aplicações em engenharia de tecidos. Devido às propriedades mecânicas, estabilidade e capacidade de mimetizar a matriz extracelular (ECM) dos tecidos nativos, hidrogéis baseados em polissacarídeos são apelativos para uso em terapias regenerativas com recurso a células. A impressão 3D é uma abordagem altamente versátil, dotando os implantes com características tridimensionais de relevo. Uma das maiores dificuldades neste campo é a escassez de materiais multifuncionais compatíveis com impressão 3D capazes de mimetizar a ECM do osso. A pectina, polissacarídeo aqui utilizado, destaca-se pela solubilidade e maior capacidade de personalização quando comparada com outros biopolímeros. Nanosilicatos podem ser utilizados para modificar o fluxo polimérico, de modo a torná-lo compatível com processos de impressão, possuindo também propriedades osteogénicas, de reforço mecânico e desencadeamento de atividade celular, compensando a falta destes atributos nos polissacarídeos.

Neste trabalho, a incorporação do nanosilicato laponite (LAP) na estrutura de pectina-metacrilada (PEMA) foi estudada. Para esse efeito, a pectina foi modificada através dum processo de metacrilação, dando origem a um hidrogel foto-reticulável. A concentração do polímero foi mantida inalterada enquanto que a do nanosilicato foi variada de modo a estudar a sua influência nas propriedades dos andaimes, assim como para definir a janela dentro da qual o compósito é imprimível. Utilizando um processo de extrusão, as composições de PEMA/LAP foram impressas e parametricamente quantificadas, tendo também sido realizado um estudo reológico. Módulos de elasticidade num intervalo de 8 a 48 kPa foram obtidos, valores considerados ideais para a osteogénese. Tanto as propriedades reológicas como as mecânicas confirmaram a existência de um limite de saturação para o nanosilicato, a partir do qual as propriedades dos andaimes se deterioram. Este nanocompósito PEMA/LAP demonstra capacidades notáveis para regeneração óssea, apresentando-se como uma alternativa barata, personalizável, biocompatível e compatível com impressão 3D.

Palavras-chave: hidrogel, andaime, impressão 3D, laponite, pectina-metacrilada, polissacarídeo, regeneração óssea

Abstract

Hydrogels have proved to be highly attractive biocompatible materials which can be used for tissue engineering applications. Among the hydrogels, Polysaccharides due to their superior mechanical properties, stability, and resemblance of the native extracellular bone matrix (ECM) are appealing to use as cell-based regenerative therapy. To impart complex 3-dimensional architectural features, printing methodology is a versatile approach due to its capability to fabricate customizable scaffolds. Pectin stands out since its solubility can be more easily modulated compared with the other natural polymers. One of the big burdens in this regard is that the lack of multifunctional printable materials which can resemble ECM of bone tissue. In order to make pectin printable for bone tissue engineering, nanosilicates can be used to modify the flow behavior of pectin. Moreover, nanosilicates provide osteogenic properties, mechanical reinforcement, and triggering of cell phenomena, making up for the absence of such properties in polysaccharides.

Here, we hypothesized that the incorporation of laponite (LAP) nanosilicates within methacrylated-pectin (PEMA) enhance the shape fidelity and mechanical properties. Therefore, pectin was modified through a methacrylation process creating a UV-crosslinkable methacrylated-pectin (PEMA) hydrogel. Polymer concentration was kept unchanged while laponite amount was tuned in order to study its influence on disc-shaped scaffolds and to define a printability window. Using an extrusion-based process, the compositions of PEMA/LAP were printed and their printability properties quantified and a detailed study on the rheological properties of the PEMA/LAP hydrogels was conducted. Remarkably, elastic modulus in the range of 8-48 kPa were obtained, which is ideal to promote osteogenesis. Rheological properties, as well as mechanical properties, confirmed the existence of a saturation limit for LAP, from which scaffolds properties deteriorate. This nanocomposite platform highlights the potential of printed PEMA/LAP for bone tissue engineering, proposing a 3D-printable, low cost, tunable, biocompatible and highly promising alternative in this field.

Keywords: hydrogel, scaffold, 3D printing, laponite, pectin-methacrylate, polysaccharide, bone regeneration

Contents

List of Figures

List of Tables

Symbols

A	Area
A_{re}	Real area
A_{te}	Theoretical area
DR	Degradation rate
ε	Strain
G'	Storage Modulus
G''	Loss Modulus
HF	Height Fidelity
H_{re}	Real height
H_{te}	Theoretical height
L	Perimeter
η	Viscosity
PR	Printability Ratio
$\mathbf{p}_v$	p-value
SF	Shape Fidelity
SR	Swelling Ratio
SPR	Spreading Ratio
W_i	Initial weight
W_d	Dry weight
σ	Stress

Acronyms

AM	Additive Manufacturing
AEMA	Aminoethyl Methacrylate
BTE	Bone Tissue Engineering
CAD	Computer-aided design
DI	Deionized water
ECM	Extracellular Matrix
FTIR	Fourier Transform Infrared Spectroscopy
GAGs	Glycosaminoglycans
LAP	Laponite
LVE	Linear Viscoelastic
MD	Methacrylation Degree
PEMA	Pectin-Methacrylate
SEM	Scanning Electron Microscope
UV	Ultraviolet

1. Introduction

1.1. Bone Tissue Engineering

Bone tissue engineering (BTE) is a highly interdisciplinary field that combines insights from both engineering and life sciences, thus increasing the complexity of successful new bone growth. To fulfill all requirements for BTE, different kinds of materials have been studied in the last decades. Traditional methods to repair bone defects like autografts, xenografts and allografts show some disadvantages, like donor-site morbidity and uncertain secondary effects [1], and have limited clinical use. Metallic implants and biomaterials like calcium phosphate, bioglass or hydroxyapatites have proven to be good alternatives, however they still lack the ability to meet all needs for complete regeneration of bone tissue, especially when it comes to biocompatibility, biodegradability and cell incorporation. So, the development of other biomaterials like polymeric scaffolds and in particular hydrogels has been intensively studied in order to overcome the limitations of today's clinical solutions for bone damage repair.

A bone scaffold must show: biocompatibility, so it doesn't trigger any inflammatory response by the organism; osteoconduction, osteoinduction, and osteogenic properties; pore size higher than 100 μm and highly interconnected; mechanical properties at least similar to the ones of the adjacent host tissue; adequate degradation profile, matching the speed of new bone generation; enough rigidity so that their structure and properties are not damaged during the required procedures and transportation before surgery; sterile environment for cell seeding; optimal integration between the implanted material and the native tissue [2].

1.2. Hydrogels for Bone Tissue Engineering

Hydrogels are some of the most exciting and promising materials for research in the biomedical field, and bone tissue engineering is no exception. Despite most of the research on these materials being carried on the biomedical field, these hydrophilic polymeric chains, that have been around since the last decade of the 20th century [3], are currently used for contact lenses and hygiene products, for instance **[8]**, and are also a research field in soft electronics and actuators [4]. They stand out due to some highly attractive properties like biocompatibility, flexibility, softness, high water content [5] and the versatility to engineer their physicochemical properties to meet the needs of each application. Consisting of chains of repeating monomers (homopolymers) or chemically different monomers (copolymers) [6], hydrogels can be applied as space-filling agents, delivery vehicles for bioactive molecules and scaffolds for wound dressing and tissue engineering, both 2D and 3D [7].

In order to meet the requirements for bone regeneration, hydrogels are tailored. By tuning their polymer concentration, crosslinking density, crosslinking mechanism and/or chemical composition [6], for example, properties like degradation rate, swelling ratio, porosity, and mechanical properties can be optimized to meet bone ingrowth needs. Besides, as 3D networks with high hydrophilicity, hydrogels provide a good environment for cells [7], making them ideal to be used as cell carriers. Its three-dimensional structures act as a mechanical support for cells and allow nutrients, oxygen, and metabolites' transport to and from the encapsulated cells [6].

Polymers in which hydrogels are based on can either be synthetic or natural (biopolymers). These can also be combined and used as composite scaffolds. Synthetic polymers show poor biocompatibility [6], however, they provide reproducible properties and chemistries since they mainly depend on the conditions of their synthesis. Biopolymers are most commonly used for tissue engineering applications since they mimic the natural extracellular matrix (ECM) of the tissues, either by being components of this matrix themselves, like collagen or by having similar macro-molecular properties [7]. This matrix is responsible for giving structure, support and regulation on different levels for the living tissue through its 3D acellular network [8], and guides remodeling of the tissue when in repair, assuring that

there is not any kind of inflammation or immune response from the organism [1]. Among biopolymers, gelatin derivatives and collagen are widely used for a variety of biomedical applications. Collagen is a structural tissue protein that provides integrin-binding sites, an essential biological cue for cell-ECM interactions. Gelatin, being a product from collagen hydrolysis, also shows great biological performance since it contains the same binding sites on its structure [6]. However, mechanical weakness and fast degradation in vivo of these proteins make them unattractive for bone regeneration [8], imposing the study of other alternatives like polysaccharides, which meet several requirements for tissue engineering [9].

1.2.1. Polysaccharide-based Hydrogels

Polysaccharides, the most abundant biomolecules in nature [9], are the polymer group with the longest and widest medical applications due to their excellent properties [10]. They have been applied in the design of multiple tissue engineering constructs like bone, neural tissue, heart valves, blood vessels, and cartilage, among others [11]. They can have vegetal, algal, microbial and animal origin [9] and their capacity to mimic the ECM of native tissues (from both chemical and physical viewpoints) has an impact on the adhesion, spreading and proliferation of cells, guiding tissue regeneration in the desired direction, thus impacting tissue regeneration success [11]. The resemblance of polysaccharide-based hydrogels to some components of bone, like the mineral binding non-collagenous proteins glycosaminoglycans (GAGs), makes polysaccharides based-scaffolds some of the most commonly used alternatives for BTE applications. GAGs are strongly hydrophilic macromolecules composed of polysaccharide chains made up of repeating disaccharide units. Many of the soluble growth factors inducing osteogenic differentiation and promoting the biosynthesis of osteogenic proteins require GAGs to facilitate their interaction with surface receptors since these components bind growth factors and cytokines. GAGs are also essential for moderating crystallization [7]. Contrary to some synthetic polymers, polysaccharides tend to avoid stimulation of chronic inflammation or immunological reactions and toxicity, which represents a huge advantage in tissue engineering [12]. Polysaccharides also show remarkable biocompatibility, biodegradability, better mechanical properties in comparison with other polymers and modifiable functional groups [11], since they usually contain hydroxyl, carboxyl, and amino groups, which can be functionalized [9].

Pectin is a naturally derived polysaccharide usually found in the cell walls of terrestrial plants and fruits [13]. It has long been used in the food and pharmaceutical industry, especially due to its gelling ability [14]. More recently, it has also played an important role in gene delivery [15,16], drug delivery [16,17], cancer therapy [19] and as a scaffold for tissue engineering [19,13]. Its thickening and gelling abilities make pectin an attractive biomaterial, as well as its biocompatibility, biodegradability, non-toxicity, and abundancy of modifiable functional groups [13]. Pectin's branched nature and the complexity of its chemical composition it's similar to alginate [20], which is one of the most used biopolymers in tissue engineering. However, in native composition, this polymer lacks cell-adhesive and protease-cleavable sites, acting as a "blank-state". Here, pectin backbone was methacrylated with aminoethyl methacrylate (AEMA), a process that consists of a direct reaction between pectin and methacrylic anhydride (see Figure 1.1), where methacrylate groups substitute carboxylic groups on pectin structure until the desired methacrylation degree (MD) (number of substituted groups) is achieved [13]. This process originates pectin-methacrylate (PEMA), a UV-crosslinkable hydrogel when associated with a photoinitiator (Irgacure D-2959). Methacrylate groups provide the ability to form covalent bonds between the polymer chains, induced by UV crosslinking. These covalent bonds

improve the mechanical properties and stability of hydrogel [21]. A schematic of PEMA crosslinking can be found further in the Discussion and Results section.

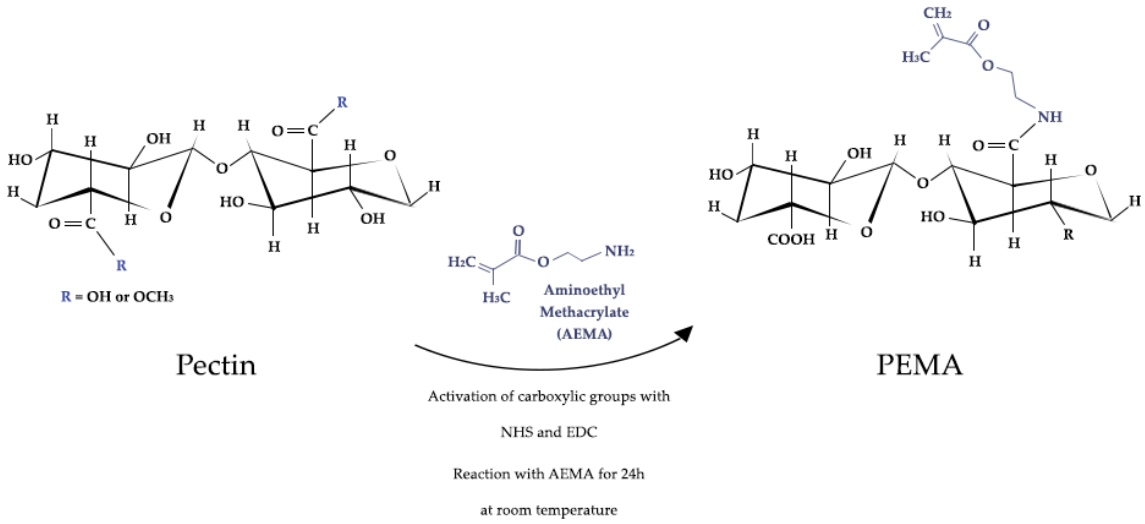

Figure 1.1 – Scheme of pectin's functionalization to obtain PEMA, with the corresponding chemical structures represented.

The parameters of photo-crosslinking (light exposure time, light intensity, light wavelength, and initiator concentration) critically influence the properties of the resulting hydrogel. Tuning of chemical, degradability, physical and mechanical properties of PEMA-based hydrogels can be done by adjusting both MD and polymer concentration, as well as crosslinking time. Higher polymer concentrations, crosslinking times and methacrylation degrees lead to stiffer scaffolds with lower degradation profiles, however, the scaffolds become too rigid and dense which highly affects, among other properties, cell viability [21]. Mehdi Mehrali et al. [13], for instance, studied the influence of MD on different properties by using PEMA hydrogels with low, medium and high MD.

Polysaccharide-based scaffolds provide good degradation profiles and show high resemblance with the ECM of the natural tissues, but lack biological cues to trigger cellular activity and send cell signals to guide morphogenesis [13]. Besides, although mechanical properties of these biopolymers might be good for some other applications, bone repair requires superior properties in that domain. In this case, PEMA on its own doesn´t allow the production of 3D constructs stiff enough for bone repair, even after crosslinking, and its viscosity it's also not enough to make it compatible with 3D printing techniques. Therefore, reinforcement strategies to overcome these limitations must be applied.

1.3. Hydrogel Reinforcement

In order to enhance hydrogels' physical, chemical and biological properties, these materials can be reinforced. Despite the great potential of hydrogels, most of the polymers, including polysaccharides, lack mechanical strength for load-bearing applications, biological cues or degrade too quickly [6]. Therefore, several reinforcing strategies are studied on a daily basis by the scientific community. For instance, some papers reported reinforcement of pectin-methacrylate with Arginine-Glycine-Aspartic acid motifs [22] or Gelin-s [13], a gelatin derivative which provides higher biological activity. Gelatin derivatives like Gelin-s or gelatin methacrylate are commonly blended with polysaccharides [13,8]. Reinforcement with inorganic materials like nanosilicates or several other kinds of nanoparticles (carbon nanotubes, graphene, bioactive glasses, hydroxyapatites) is also widely used [23,6], since not only endows biological enhancement to the hydrogels but also notably impacts mechanical, rheological

and physical properties. Reinforcement with nanosilicates, in specific, significantly impacts mechanical properties, degradation profile, flow properties and cell-scaffold interaction [6]. Some approaches as in [24] use a double reinforcement strategy, using both polymers and nanosilicates as reinforcers.

1.3.1. Nanosilicates

Silicate deficiency in our organism can cause several health issues, like osteoporosis since this trace mineral is crucial for bone health. It has been shown that silicate stimulates collagen synthesis, boosts calcification/mineralization and guides osteogenic phenomena [25]. Besides tissue engineering, nanosilicates are also well-established components for drug delivery [26,27] and wound healing applications [28]. The most common are montmorillonite, hectorite and the smectite family. Smectite family consists of hydrous materials which swell and turn into solid-plastic masses when submerged in water. Laponite (LAP), member of the smectite family, is a 2D synthetic nanosilicate with 30 nm in diameter and 1 nm in thickness that has been shown to provide enhanced physical, chemical, biological and shear-thinning properties. It has a discotic charged surface (both positive and negative charges on the surface, resulting in unique anisotropic interactions between the nanoparticles), uniform shape, high surface-to-volume ratio (enhances adsorptive behavior), and biocompatibility [28]. This nanosilicate has a 2-layer disposition, consisting of two parallel silica sheets with a magnesium oxide sheet between them. When dispersed in water, the sodium cations between layers are released, unbalancing the charge of laponite. The platelets adopt a negative charge and the edges a positive one, as long as the pH is lower than 11. With this positive charge on the edges, a "house of cards" microstructure is achieved due to the electrostatic interactions between the opposite charges of the nanoplatelets. This microstructure is responsible for the increase in viscosity and shear-thinning behavior of laponite dispersions [29]. Schematics on laponite microstructure and its behavior can be found in the Appendix, section A (adapted from [30]). These materials also act as physical crosslinking points of polymeric materials, as represented in Figure 1.2. This has an impact on properties such as swelling ratio, degradation rate, and mechanical stiffness. Moreover, imaging of the subsurface cellular process is facilitated due to the optical transparency of LAP in aqueous media [28].

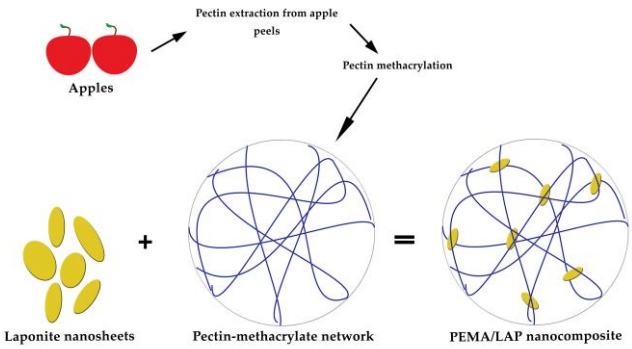

Figure 1.2 - Schematic of the nanocomposite in focus in this work, from pectin's extraction to laponite incorporation into the polymer's network.

M. Hasany *et al.* [31] extensively studied the reinforcement of alginate/hyaluronic acid hydrogels with 3 different 2D nanosilicates, including laponite, for BTE purposes. The nanoreinforced hydrogels were associated with an increase in mechanical properties, extension on cell viability for longer periods of time, expression of osteogenic markers like alkaline-phosphatase and also an increase in mineralization. The same trend was reported in [23], where laponite reinforced gelatin methacrylate scaffolds. The addition of the nanosilicate increased stiffness and *in vitro* stability. It was also noticed its effect on cell adhesion and proliferation, as well as the triggering of osteogenic differentiation of preosteoblasts, affirming the outstanding potential of laponite for bone regeneration.

1.4. **Fabrication**

1.4.1. Shear-Thinning Behavior

In order to obtain printable hydrogel compositions, optimization of their viscosity and other rheological properties is crucial. both Newtonian and non-Newtonian formulations are currently studied. Contrarily to the Newtonian ones, non-Newtonian extrusion inks show shear-thinning behavior, which means viscosity decreases with the increase in strain rate. Nanosilicate dispersions follow a non-Newtonian behavior due to their shear-thinning properties. In a nanocomposite, it is important to understand the effect of shear forces on both the polymer and the nanosilicate. Under low shear rates, the previously reported "house of cards" microstructure of laponite is adopted. However, when submitted to high shear rates, this microstructure collapses resulting in a twist in the orientation of the nanoplatelets, orienting them in the flow direction, hence decreasing viscosity. Regarding the polymer network, these shear forces result in a disentanglement of its chains, which are at rest when no external forces are being applied. These structural changes allow viscous formulations to decrease their resistance to flow when submitted to shear forces, returning to their original shape once the load is removed, which is believed to increase printing resolution [29].

For these reasons, nanosilicates have been widely used for the development of injectable biomaterials for tissue engineering. Laponite viscosity-increase capacity and shear-thinning behavior allowed the printing of gelatin methacrylate [23] and alginate/methylcellulose hydrogels [32], both using extrusion-based 3D printing, showing the outstanding ability of this nanosilicate to modulate flow properties of hydrogels.

1.4.2. Additive Manufacturing

Additive manufacturing (AM) techniques play an important role in tissue engineering, becoming the number one choice when it comes to scaffolds' production. Commonly known as 3D printing, these techniques allow the production of 3D structures according to a predesigned CAD (computer-aided design) file that can be sketched to have the exact geometry of the defect-site. 3D printing aims to fabricate 3D structures that are able to create a micro-environment where cells are able to grow, spread and differentiate, and also provide the mechanical, degradation, physical and chemical properties that the application requires. Hydrogels are widely compatible with 3D printing techniques due to their tunability since the possibility of engineering their composition by changing its concentration or adding additives that change its flow properties allows reproducibility of printing constructs [33]. It is also of paramount importance that the printing is reproducible and has good resolution and shape fidelity, i.e., the design and the built construct should be the most equivalent as possible in terms of features and dimensions. The maintenance of structural integrity after printing is also of big importance [34]. Each bioink is carefully studied and optimized until a trade-off between best properties and best printing conditions (nozzle diameter, printing speed, pressure, etc.) is achieved. The most used AM techniques for tissue engineering are micro extrusion, inkjet, laser-assisted bioprinting [33], light-mediated stereolithography and fused deposition modeling. Besides transplantation, 3D printed constructs are also believed to be ideal as *in vitro* models to study diseases, for example [34].

1.4.3. Extrusion-based 3D Printing

In extrusion-based 3D printing, 3D structures are built by dispensing bioinks through nozzles or needles. Hydrogels are highly attractive materials for this technique, due to their amazing properties. The ink is loaded into a reservoir (cartridge) and is then extruded by a piston, screw or pneumatic system until it reaches the nozzle aperture [29]. Afterward, the ink exits the nozzle and is dispensed in

a building platform which follows the x-y directions of a pre-designed CAD-file [34]. This technique allows the printing of complex shapes like bionic ears or heart valves [34,35] and is compatible with several crosslinkable hydrogels (photo, chemical or thermal) [37]. In this work, a piston-driven extrusion technique was used, and schematic of the printing system, as well as a picture of the used setup, can be seen in Figure 1.3.

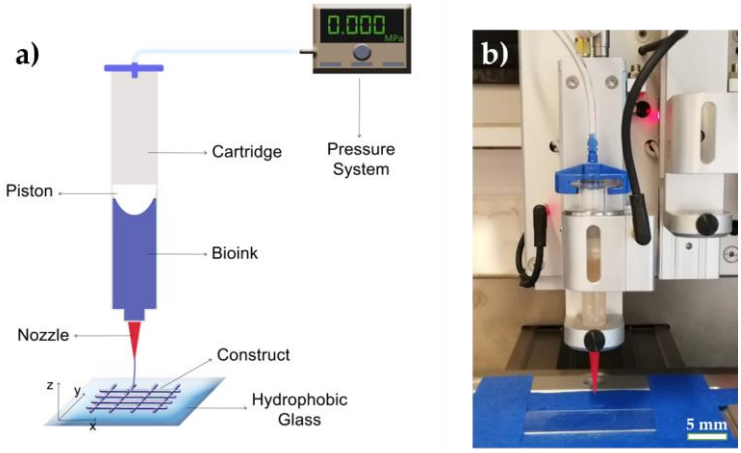

Figure 1.3 - a) Schematic with every component of the printing system; b) Actual printing setup.

Inkjet printing and extrusion-based 3D printing are the two most used AM techniques. Extrusion-based techniques are an evolution of inkjet printing, allowing higher resolutions and continuous printing of viscous substances instead of just droplets [37]. In this technique, the printed formulation should show a continuous flow while exiting the nozzle tip, exhibiting a liquid-like behavior. However, high viscosity is needed so that the ink doesn't show droplet formation due to surface-tension driven forces, as well as to keep its shape once it is printed. For that reason, shear-thinning inks are widely used for this purpose, since they go from a solid-like behavior to a liquid-like one when a shear load is applied, returning to its viscous state after printed [29].

2. Materials and Methods

2.1. Materials

Pectin was extracted from apple peels (50-75% esterification) and methacrylated (MD=15%) through the same process used in [13], which can be found in the Appendix, section B. The photoinitiator 2-Hydroxy-4'-(2-hydroxyethoxy)-2 methylpropiophenone (Irgacure D-2959) and Sigmacote were supplied from Sigma-Aldrich. Laponite RD (LAP), containing SiO_2 (59.5%), MgO (27.5%), Na_2O (2.8%) and Li_2O (0.8%) with low heavy metals content was purchased from Rockwood Additives Limited, UK. Deionized water (DI) was used for all the experiments. Cartridges, pistons, and nozzles were provided by Nordson EFD, USA.

2.2. Preparation of the Hydrogels

In this work, four compositions were studied: PEMA 2% (2P), PEMA 2%: Laponite 1% (2P1L), PEMA 2%: Laponite 2% (2P2L) and PEMA 2%: Laponite 3% (2P3L). A 0.5 wt.% Irgacure D-2959 solution was used for every composition. Laponite 1, 2 and 3 wt.% were dispersed in the photoinitiator solution, covered in aluminum foil and sonicated for 25 minutes. The solutions were then vortexed until they looked translucid. PEMA was weighted and placed inside a glass sealed bottle with a stir bar along with laponite solution (2P1L, 2P2L, 2P3L) or just Irgacure solution (2P). The bottles were covered in aluminum foil and left in a hot plate to mix for 5h at 65ºC and 50 rpm. Afterward, using a gel pipette, the solutions were loaded into a casting mold with 4 mm in diameter and 6 mm in thickness disc-shaped holes. The upper glass was coated with Sigmacote to avoid sticking and possible damage of the discs after crosslinking. The discs were crosslinked in a UV-oven (UVP CL-1000 Ultraviolet Crosslinker) for 10 minutes, with an intensity of 7 mW/cm^2 and a wavelength of 365 nm, correspondent to the absorbance of the photoinitiator. After crosslinking (except for mechanical properties and swelling ratio), the discs were put inside 1.5 ml Eppendorfs and placed in a -80ºC freezer for 2h to become lyophilized, and were then left to dry overnight in the freeze dryer.

2.3. Characterization Techniques

2.3.1. Fourier-Transform Infrared Spectroscopy (FTIR)

Fourier Transform Infrared Spectroscopy (FTIR) was performed in transmission mode for every composition (N=2), over a range of 530-4000 cm^{-1} with a 4 cm^{-1} resolution. For this purpose, a PerkinElmer Spectrum 100 FTIR spectrometer (USA) equipped with the ATR accessory was used.

2.3.2. Swelling Ratio and Degradation Rate

To measure the swelling ratio (SR) of the hydrogels, N=3 discs were weighted in the following time points: 1h, 2h, 4h, 8h, 24h, 48h, 7 days, 14 days and 21 days. The discs were put in a 24 well-plate and SR was calculated as the coefficient between the initial dry weight of the disc (W_i) and the swollen weight at a specific time point (W_s). Before weighting, the excess of water was removed with a paper filter.

Degradation rate (DR), N=3 samples were used for each time point (1, 2, 7, 14 and 21 days). At each time point, the samples were taken out of the 24 well-plate, freeze-dried overnight and weighted in the following day. DR was obtained by dividing the weight of the dried degraded scaffolds at each time point (W_d) by its initial weight (W_i).

For both techniques, the media was changed every two days.

2.3.3. Porosity Study

N=2 discs were freeze-dried, vertically cross-sectioned and then coated with gold (Au, 6 nm) prior to Scanning Electron Microscope (SEM) imaging. A Phenom Pro Desktop SEM was used to analyze the cross-sectioned scaffolds. ImageJ software (National Institute of Health) was then used to measure the pore size.

2.3.4. Mechanical Properties

Compressive and cycle tests were performed using a Discovery DMA 850 from TA Instruments. N=4 samples were used for both tests. After crosslinking, the samples were submerged in PBS the night before compression in order to swell. The elastic modulus was calculated by analyzing the slope of the 10-15 % strain region of the Stress (σ)-Strain (ε) curve, while strength and toughness were defined as the maximum stress and the area under stress-strain curves, respectively. The samples were submitted to a strain up to 30% at a rate of 0.4 mm/min, with a load cell of 18N. For cyclic tests, these same conditions were applied to the discs for N=5 cycles. The setup can be found in the Appendix, section C.

2.3.5. Rheology Study

Rheology tests were performed on the 4 groups using a Discovery Hybrid Rheometer HR-2 from TA Instruments using a plate-plate geometry (40 mm diameter) at 25°C. Viscosity, storage modulus (G') and loss modulus (G'') were measured. Firstly, steady shear experiments were performed in order to evaluate the shear-thinning behavior of PEMA and PEMA-LAP solutions at 25°C. Flow sweep experiment with a shear rate ranging from 0.01-100 s^{-1} was applied, with a 300 μm gap size. Moreover, in order to determine the linear viscoelastic region (LVE), amplitude sweep was performed from 0.01 to 100 Pa at a fixed angular frequency of 1 rad/s. The setup can be found in the Appendix, section D.

2.4. 3D Printing

2.4.1. Printing Methodology

To determine which compositions were printable, the hydrogel inks were first loaded into 3CC cartridges, coupled with a piston and a conical 25G nozzle was attached. Afterward, the cartridges were covered in aluminum foil to avoid undesired crosslinking and connected to the pressure system of the RegenHU 3D Discovery extrusion-based bioprinter. A glass coated with Sigmacote was used as a print bed. The constructs were printed with a pressure of 0.08 MPa and at a speed rate of 8 mm/s.

2.4.2. Printing Quantification

In order to quantify the printability of the printable inks (2P2L and 2P3L), printability ratio (PR), spreading ratio (SPR) and shape fidelity (SF) were evaluated. For this purpose, square grid constructs (1 cm x 1cm) were printed with three different inner square sizes (1, 2, and 3 mm). To evaluate the printability of stacked constructs, squared hollow constructs (0.5 x 0.5 cm) with 5, 10 and 20 layers were also printed. All the pictures were taken using an Olympus SZ61 stereoscope and analyzed with ImageJ software (National Institute of Health).

2.5. Statistical Analysis

Data statistical analysis was performed using GraphPad Prism (San Diego, USA). The significant differences among the grouped data sets for swelling ratio, degradation rate porosity, mechanical properties and printability parameters (except PR) were evaluated through one-way ANOVA, followed by Tukey's post hoc test. Type 1 error rate was set to 0.05, and the statistical significance was specified as *($p<0.05$), **($p<0.01$), ***($p<0.001$) and ****($p<0.0001$). ns means the groups' difference was not significant. A table with all the p values can be found in the Appendix, section E.

3. Results and Discussion

This dissertation's main goal was to study laponite's concentration effect on pectin-based hydrogels. Having that in mind, PEMA concentration was kept at 2 wt.% while LAP was added with 1, 2 and 3 wt.%, as mentioned in the previous section. Disc-shaped scaffolds of every composition (2P, 2P1L, 2P2L, and 2P3L) were then submitted to a range of characterization techniques, such as FTIR, swelling and degradation studies, compressive tests, porosity determination, and rheology study. Afterward, a printability window was defined and the printable compositions were quantified in terms of printability ratio, spreading ratio, shape fidelity and high fidelity. The outcome results of these techniques, as well as a discussion on them, can be found in this section.

3.1. Chemical Characterization

3.1.1 FTIR

In order to verify the differences between non-crosslinked and crosslinked PEMA, FTIR analysis was performed in transmission mode, over a range between 500 and 4000 cm^{-1}. A transmittance spectrum was also obtained for all laponite groups so that the nanosilicate influence could be studied. For every group, 2 scaffolds were analyzed in 2 different regions. However, that didn't have any influence on the obtained spectra, since all of them looked similar. Despite the fact that the analysis was performed between 500 and 4000 cm^{-1}, the region from 2000 to 4000 cm^{-1} was considered to be useless for the analysis, since it didn't show any significant peaks.

In Figure 3.1, one can find the spectrum of crosslinked PEMA along with the one of non-crosslinked PEMA, right below. It must be noted that dashed lines correspond to pre-crosslinking peaks, while solid lines correspond to post-crosslinking ones.

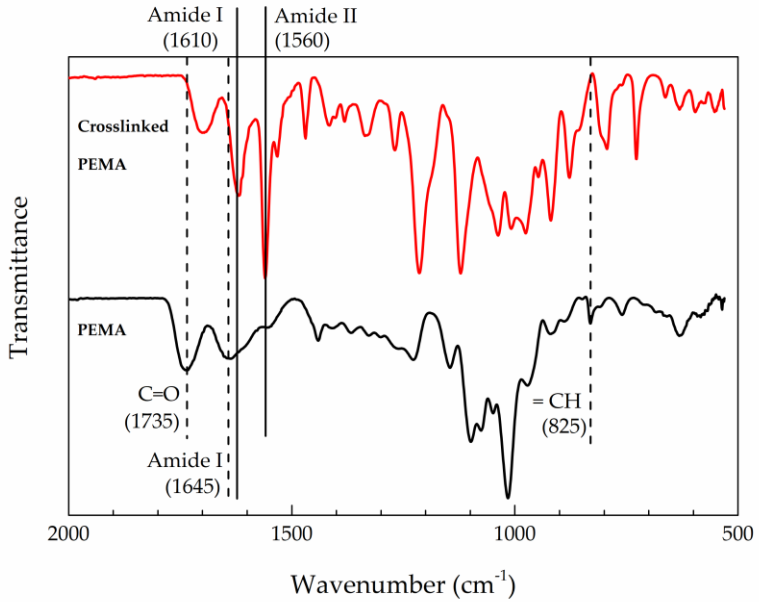

Figure 3.1 – FTIR spectra for PEMA, before and after crosslinking.

It must be noted that FTIR analysis was highly supported on the work done by M. Mehrali *et al*. [13] since PEMA was synthesized in the same laboratory (Department of Health Technology, Technical University of Denmark) and under the same conditions. As in this work, PEMA 2% was also submitted

to FTIR analysis and the peaks from Amide I, Amide II and ■CH from acrylate groups were identified and analyzed.

Firstly, starting with the non-crosslinked PEMA, i.e., in its lyophilized state, a first peak is present at 1735 cm^{-1}, which corresponds to the vibrations of the C■O bonds of this polymer. Right next to this peak, at 1645 cm^{-1}, one can find on the bottom spectrum a peak corresponding to Amide I, which shifts to 1610 cm^{-1} for crosslinked PEMA. This shift was also reported in [13]. Amide II peak was not really visible for non-crosslinked PEMA, despite a small step being present in the spectrum in that region. However, after crosslinking we can clearly see a peak at 1560 cm^{-1}, which is in accordance with [13], that reported Amide II pre and post crosslinking peaks at 1544 cm^{-1}. Amide I and Amide II transmittance peaks can be found within the band of 1500–1800 cm^{-1}, as it states in [38], and are attributed to vibrations of C ■ O and N-H bonds, respectively [39]. Lastly, it is also possible to observe a peak at 825 cm^{-1} for non-crosslinked PEMA, which corresponds to the vibration of ■CH belonging to the acrylate groups. As expected, this peak was extinct after crosslinking, since these double bonds were broken. All of these changes can be made explicit by analyzing Figure 3.2, which shows the difference between PEMA's structure before and after UV crosslinking. The chemical scheme presented in black on the left represents pectin structural bonds.

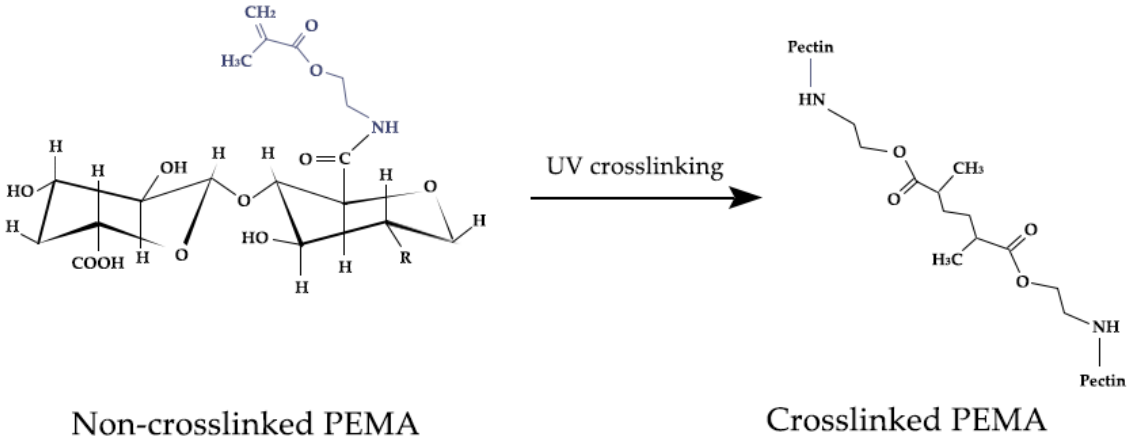

Figure 3.2 – PEMA's UV-crosslinking scheme, with the correspondent changes in its chemical structure.

In Figure 3.3 one can find the spectra for all laponite compositions (2P1L, 2P2L, and 2P3L), as well as laponite transmittance spectrum and the one correspondent to 2P, that was discussed in the previous paragraph.

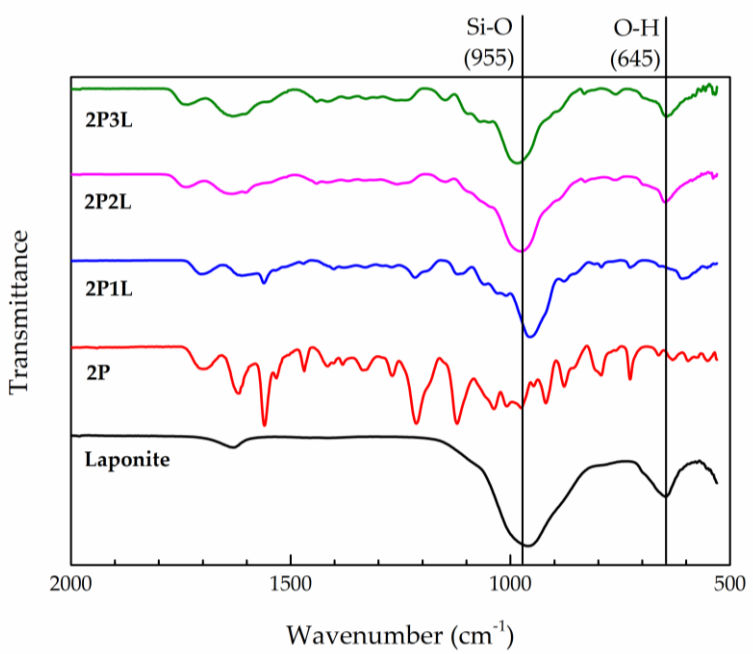

Figure 3.3 - FTIR spectra for laponite, 2P and laponite groups (2P1L, 2P2L and 2P3L).

By analyzing laponite spectrum, it is easy to notice two main peaks: one around 955 cm^{-1} and a second one at 645 cm^{-1}. The peak at 955 cm^{-1} slightly shifted to a higher wavenumber on 2P3L and 2P2L spectra, which might indicate a stronger interaction between the nanosilicate and the polymer. *G.* R. Mahdavinia *et al.* [40] studied hydroxypropyl methylcellulose-g-poly(acrylamide)/Laponite RD nanocomposites for drug release, and the FTIR analysis showed a peak related to Si–O stretching at 996 cm^{-1}. Also, a peak within the same range as the one present in laponite groups spectra was exhibited for alginate/hyaluronic acid/laponite hydrogels in [31], which confirms that it belongs to laponite, more specifically to silicon monoxide stretching. Regarding the second peak at 645 cm^{-1}, [41] reported a peak at 661 cm^{-1} on its FTIR analysis of Laponite-derived porous clay heterostructures, which was associated with O-H bending vibrations. Once again, 2P1L peaks exhibited lower wavenumbers, due to a weaker interaction between PEMA and LAP.

Moreover, one can see that laponite spectra seem to mask some of the peaks exhibited by PEMA. This is evident in the 1100 – 1600 cm^{-1} range. Transmittance decrease happened for most of the peaks, and some of them were even completely erased. Take as an example the Amide II peak, which goes from being extremely evident in the 2P spectrum to practically non-existent on the 2P3L one.

3.2. Hydrogel Stability

It was hypothesized that the incorporation of a nanosilicate would not only decrease the swelling of the hydrogels but also contribute to a slower degradation profile, due to the ability of this nanosilicate to form physical crosslinking points along the polymer's network, hence increasing their stability. In order to assess that, both swelling ratio and degradation studies were performed over a period of 21 days. Stereoscope pictures of the freeze-dried scaffolds, i.e., dehydrated, used for both studies can be found in Figure 3.4.

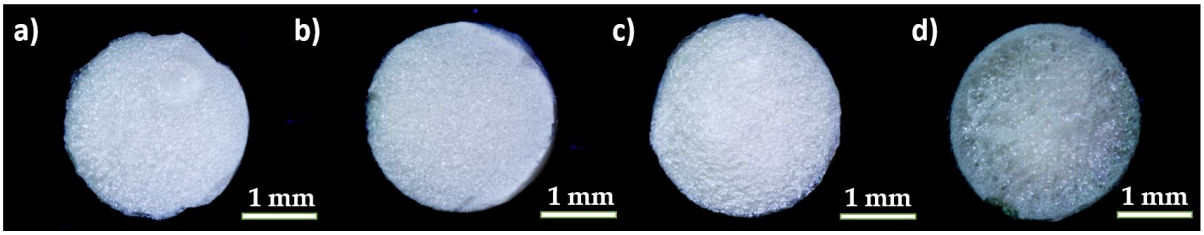

Figure 3.4 – Stereoscope photographs of freeze-dried discs corresponding to a) 2P, b) 2P1L, c) 2P2L, and d) 2P3L.

3.2.1. Swelling Ratio

The hydrophilic behavior was clearly present in PEMA and PEMA/LAP hydrogels, as can be seen in Figure 3.5**,** which refers to the swelling study carried out in this work. SR, a dimensionless ratio, was calculated by following equation (3.1), and represents the swollen mass at a specific time point (W_s) compared to the initial dry weight (W_i):

$$SR = \frac{Ws - Wi}{Wi} \quad (3.1) \qquad [13]$$

By analyzing the data, we can confirm that laponite had a noteworthy impact on the swelling ratio of the discs. As expected, the differences were more significant when comparing 2P with 2P3L, the group with the highest nanosilicate concentration. This proportionality between the increasing of LAP concentration and SR was supported by the p values obtained through the statistical analysis. 2P showed a significance of * when compared to 2P1L (p_v=0.0104), increasing to *** and *** for 2P2L (p_v=0.0003) and 2P3L (p_v<0.0001), respectively. After 21 days submerged in DI water, 2P samples showed a SR of 28.4 ± 0.7. When comparing 2P with the laponite groups, we can see a decrease of approximately 12% for 2P1L (25.2 ± 0.5), 20% for 2P2L (22.8 ± 0.9) and 26% for 2P3L (20.9 ± 0.9). In this case, the swelling of the polymer's network can be attributed to the presence of hydroxylic (-OH), carboxylic (-COOH) and amidic (-CONH-) groups in PEMA, as it states in [42]**.**

Moreover, most of the hydrogel swelling usually occurs during the first 8 to 10 hours of submersion, tending to stabilize after that period of time. This trend was followed by all groups, as it can be noticed by looking at the correspondent graph (Figure 3.5). For the first 8 h, 2P exhibited a SR of 26.6 ± 0.8, meaning that 93% of the swelling occurred during this period. As expected, laponite compositions showed a smaller swelling percentage for the same amount of time. During the first 8 hours, 2P3L hydrogels registered 84% of their swelling, while the 2P2L ones registered 81%. 2P1L registered the lowest value of them all, with a swelling percentage of 76%. Nevertheless, all of the groups showed 75% of the total swelling during this period.

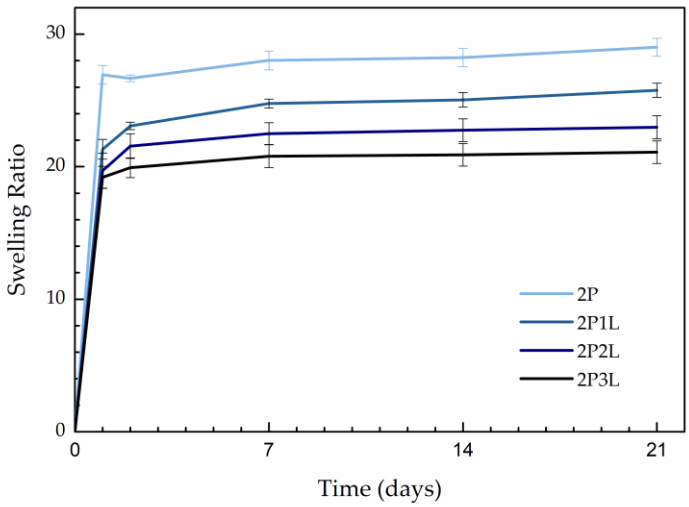

Figure 3.5 - Swelling Ratio of 2P, 2P1L, 2P2L and 2P3L hydrogels.

3.2.2. Degradation Rate

The determination of the degradation profile of a scaffold is also vital to determine its stability. Here, the degradation rate was calculated by using equation (3.2), that compares the initial dry weight (W_i) with the registered dry weight at a specific time point (W_d):

$$DR = \frac{Wi - Wd}{Wi} \times 100 \quad (3.2) \qquad [13]$$

In Figure 3.6 one can find the degradation profiles of the studied hydrogel nanocomposites over 21 days. Although during the first 10 days the results seem highly similar among the 4 groups, after 3 weeks it is clear that they do have different degradation behaviors after all.

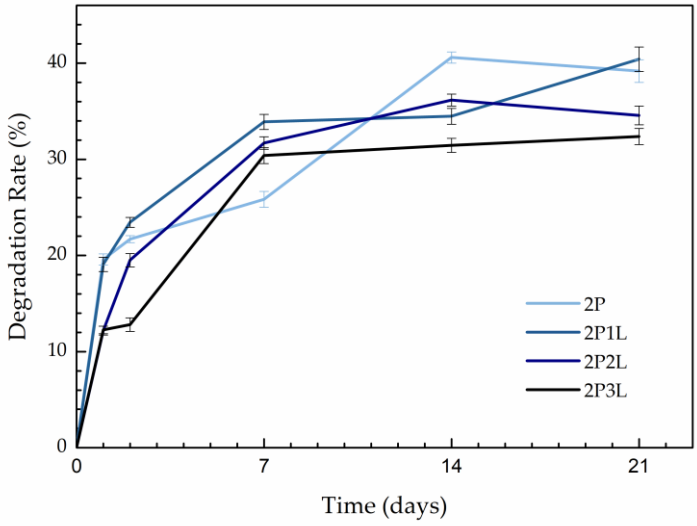

Figure 3.6 - Degradation profiles of 2P, 2P1L, 2P2L and 2P3L hydrogels.

This discrepancy was more perceptible between 2P, 2P2L, and 2P3L since 2P1L exhibited a not-significant difference comparing to 2P, as it can easily be concluded by looking at the graph above and double-checked by examining its p-values. 2P vs 2P2L showed differences with a significance of * (p_v=0.0103), significantly increasing to *** for 2P3L (p_v=0.0004).

The discs only made from PEMA showed a degradation of 39.2 ± 1.2% after 21 days in DI water, while the ones with 2 and 3 wt.% LAP exhibited degradation values of 34.6 ± 0.9% and 31.3 ± 0.8%, respectively. These results remark the outstanding abilities of laponite.

3.3. Porosity Study

Porosity is a parameter of big importance for BTE, since it regulates the diffusion and transport of substances in and out of the scaffold, like nutrients and waste, by adjusting the scaffold's permeability. It also impacts cell spreading and proliferation when these are seeded inside the hydrogel network. Hannink *et al.* [1] states that 100 μm is the minimum recommended pore size, since it allows a good transport of waste, oxygen, and nutrients within the scaffold, while pores above 300 μm are capable of enhancing osseointegration of the implant after surgery, as well as osteogenesis, oxygenation and vascularization (angiogenesis) since a larger surface area results in higher ion exchange. To study laponite's effect on the pore size of the scaffolds, SEM analysis was performed.

In Figure 3.7 one can find SEM pictures of the 4 studied compositions. These pictures correspond to carefully vertically cut cross-sections of the freeze-dried scaffolds. Following Au deposition to enhance imaging abilities, the cross-sections were observed with a desktop SEM. ImageJ was used to measure the pore size.

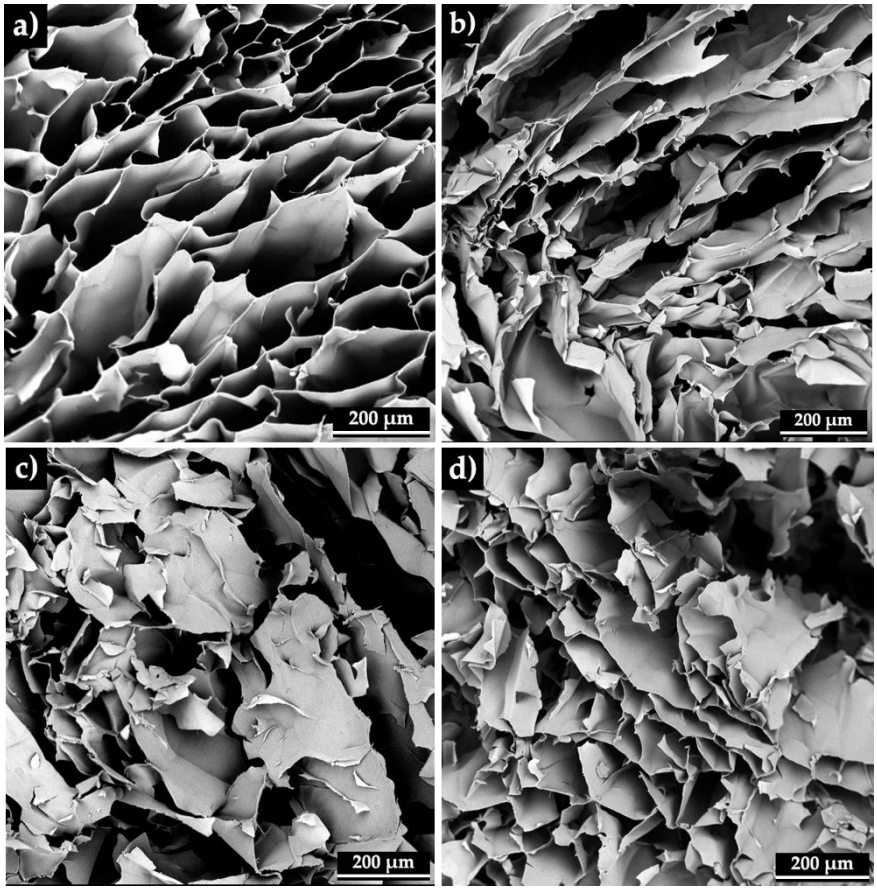

Figure 3.7 - SEM pictures displaying the pore size of a) 2P, b) 2P1L, c) 2P2L and d) 2P3L lyophilized scaffolds.

By looking at the pictures, one can observe that the first one, corresponding to 2P, exhibits an organized pore network. A similar organization was shown by pectin scaffolds with different

methacrylation degrees in [13]. However, this organization was partially lost for the laponite compositions, accompanied by a decrease in pore size.

Statistical analysis showed that 2P2L and 2P3L pore sizes were significantly different from the one exhibited by 2P, showing a significance of * (p_v=0.0143) and *** (p_v=0.0007), respectively. While 2P showed a pore size of 196 ± 103 μm, 2P2L exhibited pore sizes with an average of 107 ± 41 μm. For the scaffolds with a higher amount of laponite, the average was 78 ± 22 μm, as displayed in Figure 3.8. Besides the clear decreasing of pore size with the increasing of LAP, it was also noticeable a variation of the standard deviation (SD) for the different compositions. SD represents the diversity of pore sizes within each composition, which is considered to be of paramount importance for bone ingrowth. Comparing the compositions with 0 and 3 wt.% LAP, SD decreased from 103 μm to 22 μm, which implies that laponite incorporation had an impact on the obtained pore size range. Notably, all the groups but 2P3L exhibited an average pore size higher than 100 μm, which is considered to be the minimum recommended value for bone regeneration, as mentioned previously.

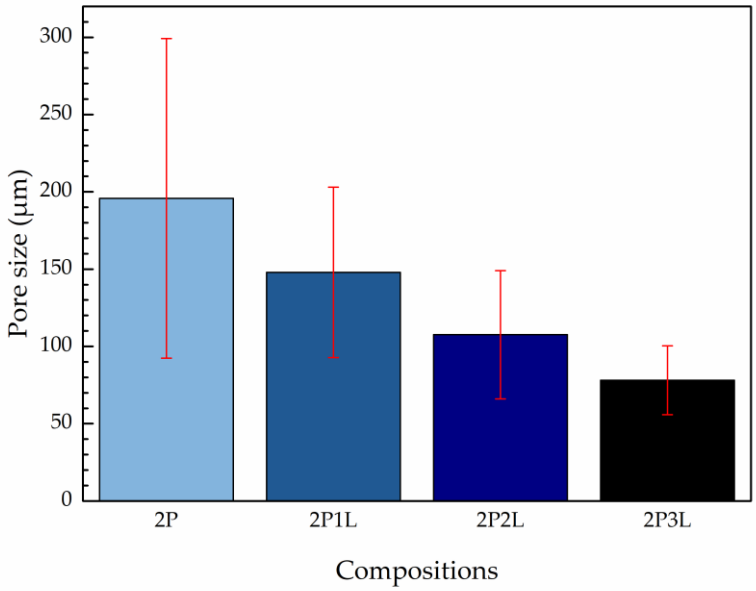

Figure 3.8 – Bar chart displaying the different pore sizes of the studied groups.

3.4. Mechanical Properties

In order to assess laponite's effect on mechanical properties, casted scaffolds were submitted to both compression and cycle tests. It is believed that the compressive load can be transferred to laponite nanoplatelets when these interact with a polymer network, increasing hydrogel stiffness. Hydrogels' mechanical properties are of big importance for bone regeneration since the scaffolds should be rigid enough to uptake the *in vivo* loads of bone microenvironment.

3.4.1. Compression Tests

In this sub-section, elastic modulus, toughness and compressive strength values for the different groups were displayed and posteriorly discussed.

Elastic modulus was considered to be the slope of the SS curves (Figure 3.9) in the 10-15% strain region, and its values can be found in Figure 3.10. This region was chosen since after 15% strain the stress increased more steeply, showing a curved profile.

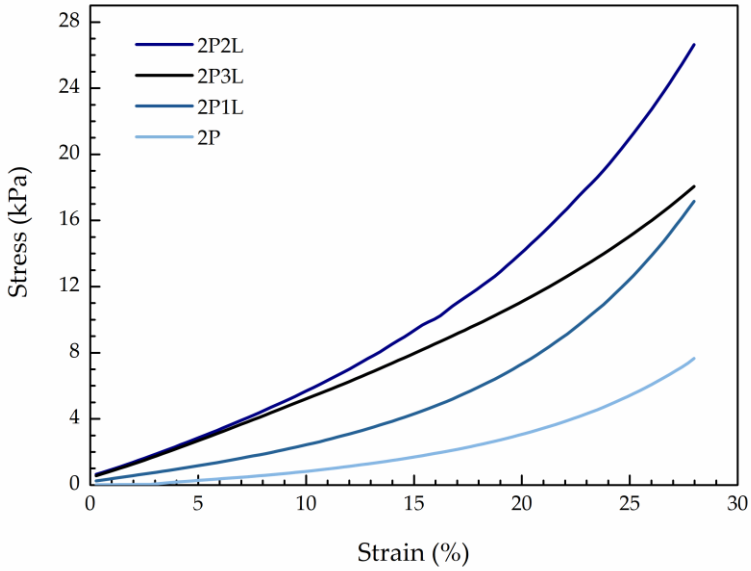

Figure 3.9 – Stress-Strain compression curves, up to 30% strain, for each composition.

Also known as Young's Modulus, elastic modulus quantifies the resistance of a material to elastic deformation, where ε and σ are directly proportional. The statistical analysis supported the comparison of 2P with laponite compositions. 2P vs 2P1L showed a significant difference of * (p_v=0.0242), while for higher laponite concentrations (2 and 3 wt.%) a significance of **** (p_v<0.0001) was reported.

PEMA 2 wt.% showed an elastic modulus of 8.8 ± 0.5 kPa, whereas 2P1L reported a value of 19.5 ± 0.8 kPa, meaning that the incorporation of 1 wt.% laponite more than doubled the modulus' value. 2P2L and 2P3L showed a 5 and 6-fold-increase in elastic modulus compared to the merely polymeric scaffolds, both reporting values of more than 40 kPa (42.0 ± 0.7 kPa and 48.1 ± 0.7 kPa, respectively). Even though 2P3L showed the higher Young's Modulus among all compositions, one can notice that the modulus increasing, when compared to the prior group (2P2L), was not as noteworthy as it was for 2P → 2P1L and 2P1L → 2P2L transitions. For instance, 2P1L vs 2P2L showed a significant difference of **** (p_v<0.0001), while 2P2L and 2P3L were the only compositions that showed no statistical significance between each other.

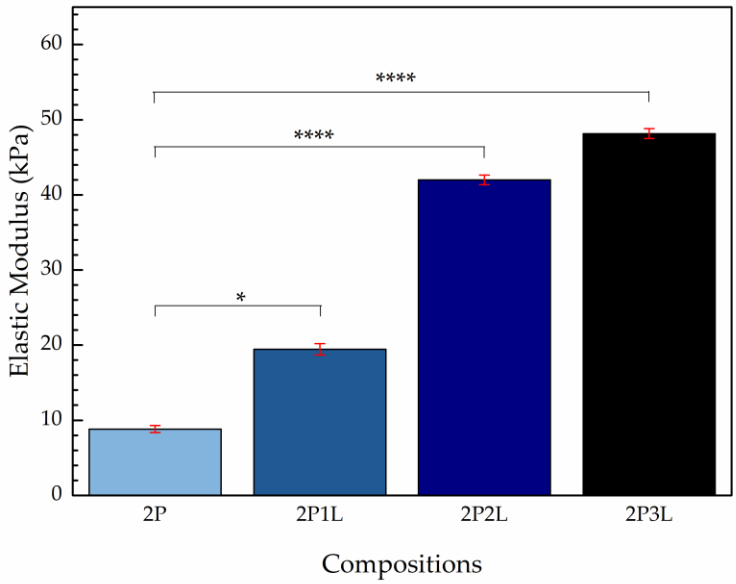

Figure 3.10 - Bar chart showing elastic modulus for each composition.

Toughness quantifies the ability of a material to absorb energy before rupture. However, since the scaffolds were not compressed until their rupture, in this work toughness corresponded to the absorbed energy at 30% strain. Statistical analysis showed that 2P was only comparable with 2P2L and 2P3L, showing significant differences of * (p_v=0.0254) and ** (p_v=0.0052), respectively. Toughness values of the studied compositions can be found in Figure 3.11. The 4 figures on the right (b), c), d) and e)) correspond to the SS curves, which have previously been shown. Toughness was retrieved from these areas under the stress-strain curves.

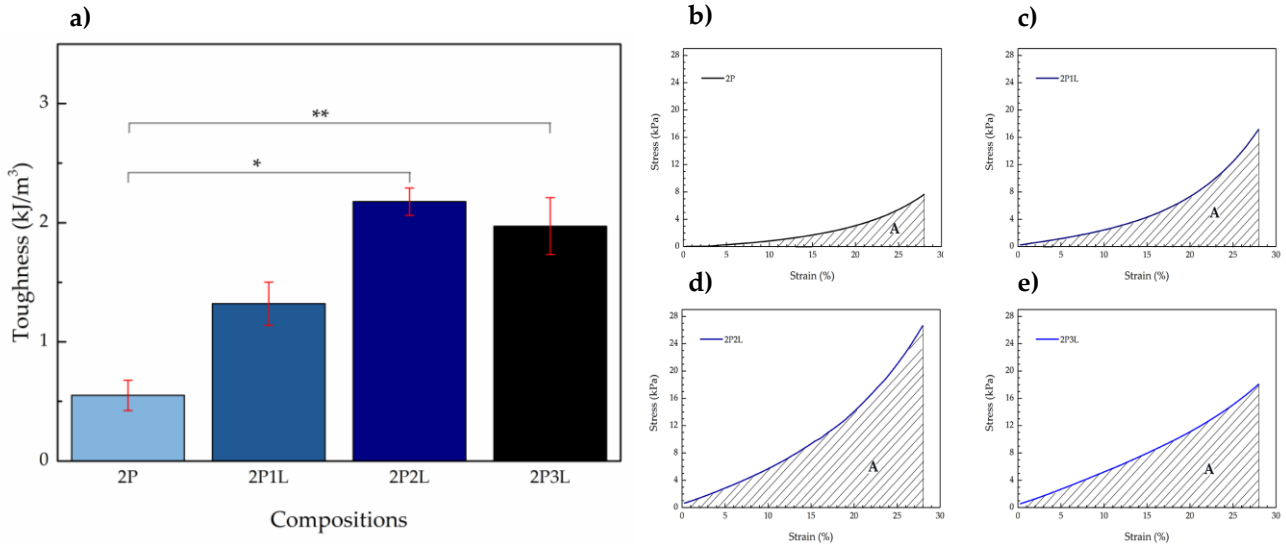

Figure 3.11 – a) Bar graph with the correspondent toughness for each composition; b-e) Area under SS curves for b) 2P, c) 2P1L, d) 2P2L and e) 2P3L.

The reinforcement of the hydrogels with 2 wt.% LAP resulted in an outstanding toughness increasing when comparing to 2P, from 0.6 ± 0.1 kPa to 2.2 ± 0.1 kJ/m^3. However, this proportionality between toughness and laponite concentration was not followed by 2P3L, which showed a value of 1.9 ± 0.2 kJ/m^3. Just to complement toughness analysis, one can observe the area under the SS curves of each composition, represented on the right side of Figure 3.11. It is evident that the area under them increases from 2P (b)) to 2P2L (d)), significantly decreasing afterward for 2P3L (e)).

Lastly, strength represents the ultimate stress before the specimen's failure. However, due to reasons that were already explained, strength was defined as the maximum σ of the compression test, i.e., the stress registered for 30% strain. The obtained strengths for PEMA and PEMA/LAP discs can be found in Figure 3.12.

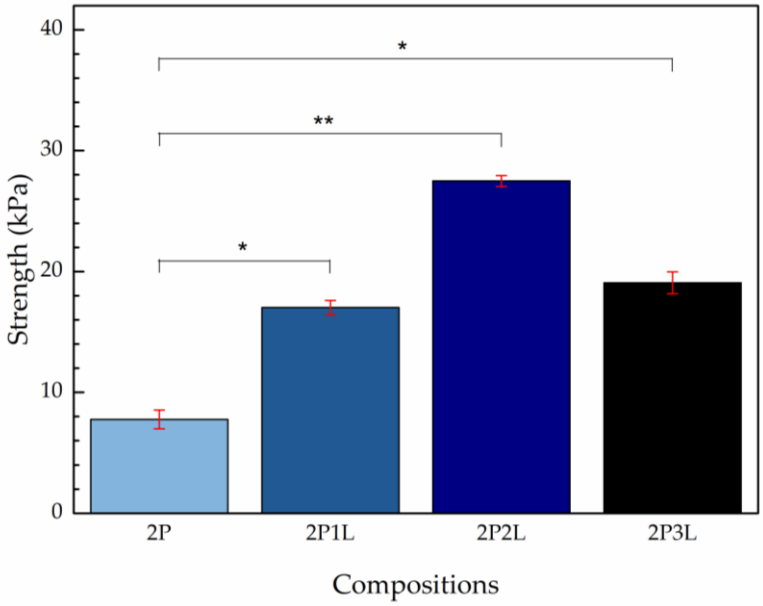

Figure 3.12 – Bar graph displaying strengths for all compositions.

As it happened for elastic modulus and toughness, one can notice that laponite had a remarkable impact on scaffolds' strength. Laponite groups showed significant differences when compared with 2P, as can be seen by the horizontal bars in the above figure. A significance of * was registered for 2P1L (p_v=0.0442) and 2P3L (p_v=0.0375), while 2P2L exhibited ** (p_v=0.0025) instead.

The incorporation of 1 wt.% resulted in a 10-unit increase in strength (from 7.8 ± 0.8 kPa, the value exhibited by 2P, to 17.0 ± 0.6 kPa). This increasing trend was followed by 2P2L, which exhibited a stress of 27.5 ± 0.5 kPa at 30% strain, while a significant fall was registered for 2P3L, exhibiting maximum stress of 19.1 ± 0.9 kPa, really similar to 2P1L's value.

3.4.2. Cyclic Tests

5 cycles of compression were performed for 4 discs of each composition. The SS cyclic compressive curves can be found in Figure 3.13.

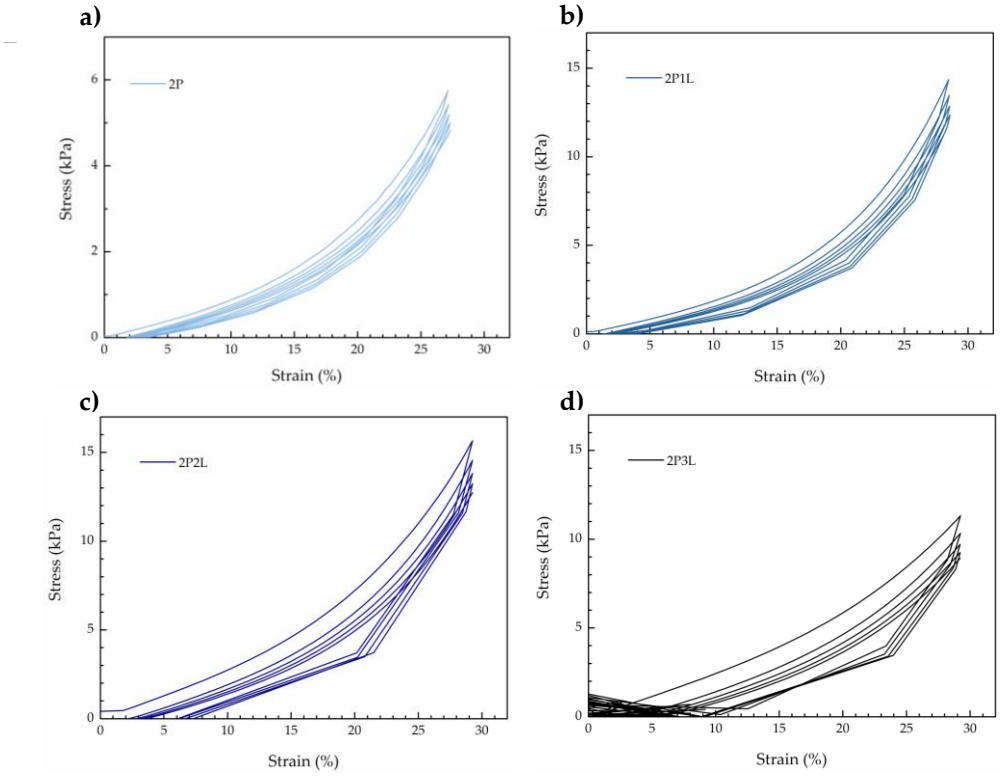

Figure 3.13 – SS compressive curves of the performed 5 cycles for all compositions.

Firstly, in order to evaluate the impact of these 5 cycles, the decrease in strength from the 1st to the 5th cycle was analyzed. The maximum σ for both cycles, for all compositions, is presented in Figure 3.14 a). For both cycles, the increase in strength among compositions followed the same behavior that was shown by PEMA and PEMA/LAP hydrogels in the previous section (see Figure 3.12). Strength

a)

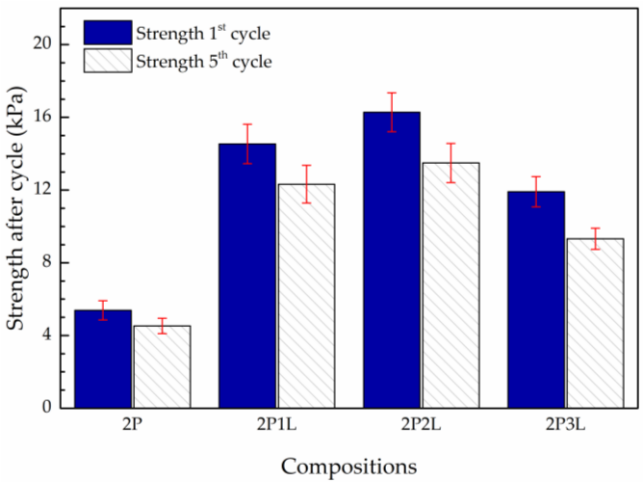

b)

Compositions	2P	2P1L	2P2L	2P3L
Strength Decrease (kPa)	0.9	2.2	2.8	2.6

Figure 3.14 – a) Bar chart showing the obtained maximum stress (strength) after 1st and 5th cycles, for each composition; b) Table displaying the differences between the obtained strengths, for each composition.

proportionally increased with laponite concentration until 2 wt.%, decreasing afterward for the last composition (2P3L). More than looking at these values, it is of bigger importance to quantify the loss in strength between cycles. Laponite groups exhibited a higher decrease in strength, with 2P2L exhibiting a decrease 3 times bigger than 2P, as one can see in Figure 3.14 b).

This may have arisen from the higher brittleness of the scaffolds owing to nanosilicate incorporation. This was also noticeable by looking at the cyclic SS curves, especially 2P2L and 2P3L, that showed a much-pronounced hysteresis.

To complement this analysis, the registered energy loss for the different compositions during the 1st cycle was analyzed. This loss corresponds to the difference in toughness between the loading and unloading curves, as represented in Figure 3.15 a), in which the red lines correspond to loading curve and the black lines to the unloading one. The dissipated energies, or energy losses, are represented in Figure 3.15 b). The 1st cycle SS curves can be found in the Appendix (section F).

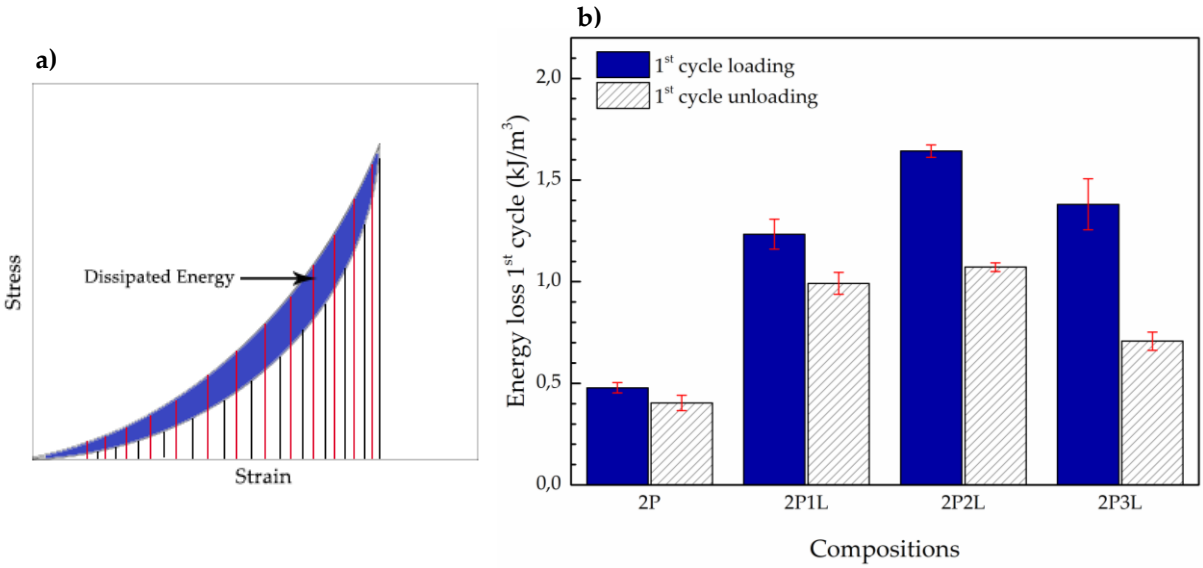

Figure 3.15 – a) Schematic representing energy Loss retrieving. b) Bar chart displaying the values of lost energy for all compositions during the 1st cycle.

By looking at the graph, it is clear that LAP incorporation significantly impacted the energy loss of the hydrogel discs. This might be explained by the adsorption capacity of laponite nanoplatelets. 2P registered the undermost loss among all groups (0.07 ± 0.02 kJ/m^3), as expected. For laponite groups, the amount of dissipated energy proportionally increased with nanosilicate content, which means that these nanoplatelets indeed adsorb some of the load energy. When compared to 2P, 2P1L exhibited a 3-fold increase (0.24 ± 0.04 kJ/m^3), surpassed by an 8-fold increase for 2P2L (0.57 ± 0.03 kJ/m^3). Once again, the nanocomposites reinforced with laponite 3 wt.% showed a stagnation. However, if compared with 2P, a 9.5-fold increase was achieved.

3.5. Rheology Study

In order to assess laponite's influence on rheological properties, a rheology study was carried out. Viscosity (η), storage modulus (G') and loss modulus (G'') of each group were obtained and discussed.

Figure 3.16 shows 4 glass bottles, turned sideways, each one of them with one of the studied hydrogel solutions.

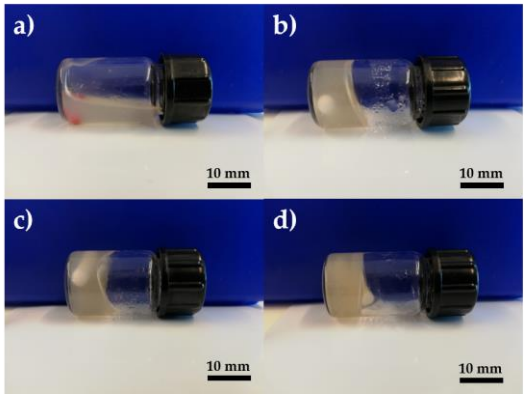

Figure 3.16 – Glass bottles with a) 2P, b) 2P1L, c) 2P2L and d) 2P3L solutions.

It is clear that the viscosity of the different solutions increased with laponite concentration. In Figure 3.16 a), which corresponds to 2P, the gel completely slipped, indicating that the solution had a liquid-like viscosity. The more laponite was incorporated into the solutions, the less they moved towards the cap of the bottle since their viscosity dramatically increased. Viscosity can be seen as the resistance of a fluid to flow.

In order to complement this visual assessment with some scientific analysis, a flow sweep experiment was performed to quantify viscosity as a function of shear rate, for the different groups. This analysis, represented in Figure 3.17, was also used to observe the supposed shear-thinning behavior of laponite compositions.

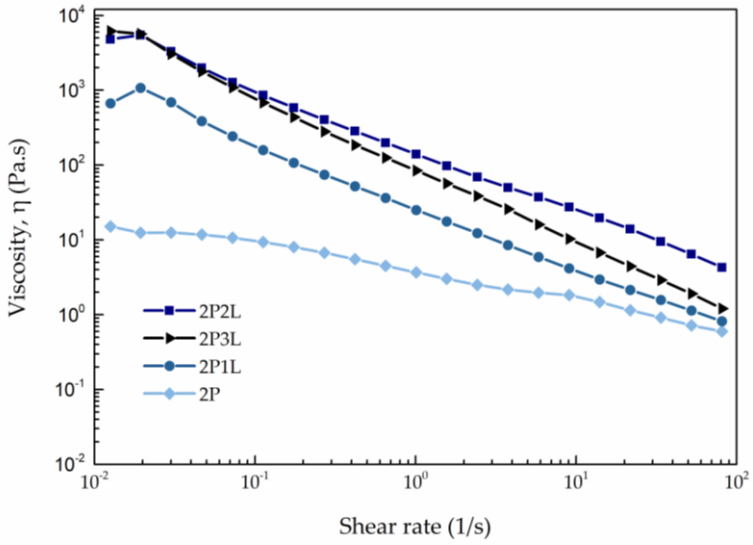

Figure 3.17 - Viscosity (η) of 2P, 2P1L, 2P2L and 2P3L in function of shear rate.

As previously mentioned, Non-Newtonian extrusion inks exhibit a shear-thinning behavior, i.e., show a decrease in their viscosity when a shear load is applied, returning to its original state when this external stimulus is removed. This behavior is only present in Non-Newtonian inks, and the addition of laponite has proven to provide this kind of flow properties to hydrogels.

At rest, 2P exhibited a viscosity around $1.5x10^1$ Pa.s. The incorporation of laponite 1 wt.% lead to an one order of magnitude increase since 2P1L showed a η of approximately $7x10^2$ Pa.s. Higher concentrations of nanosilicate registered even more astonishing increases, reporting viscosities around 5 and $6x10^3$ Pa.s for 2P2L and 2P3L, respectively. Regarding the shear-thinning properties of LAP, one can see that LAP groups dramatically decreased their viscosities with the shear rate increase, thus proving to have such flow behavior. Comparing η values for minimum and maximum shear rate, PEMA 2% discs showed a 25-fold decrease, while laponite groups exhibited fold-decreases of 811, 1117 and 5137 (2P1L, 2P2L, and 2P3L, respectively). [29] reported a similar shear-thinning behavior for alginate/laponite hydrogels, with LAP concentrations up to 6 wt.%.

In order to determine the linear viscoelastic region of the studied hydrogels, an amplitude sweep experiment was performed. Viscoelastic behavior can be divided into two portions: the elastic one, which describes the solid-state behavior of the hydrogel, represented by *G'* or G prime; the viscous one, which describes the liquid-state behavior, represented by *G''* or G double prime. LVE can be retrieved from the constant regions of both storage modulus and loss modulus graphs [29].

Starting with the storage modulus one, represented in Figure 3.18, one can notice that laponite compositions exhibited higher G', as expected. Laponite nanoplatelets tend to absorb some of the energy while the hydrogel is deformed, which is then used to induce microstructural changes to regain its original shape once the shear load is removed. The same thing cannot be said for PEMA 2%, which does not have this ability due to the lack of load-absorbing sites, which results in a smaller G prime and a shorter LVE region, that subsequently ends up in an earlier flow, as it will be discussed further in this section. Also, the value of *G'* at the plateau region corresponds to the value of rigidity of the hydrogel, which means that 2P2L proved to be the most rigid group. This is in accordance with the previously shown viscosity analysis, where this group also showed to be the most viscous.

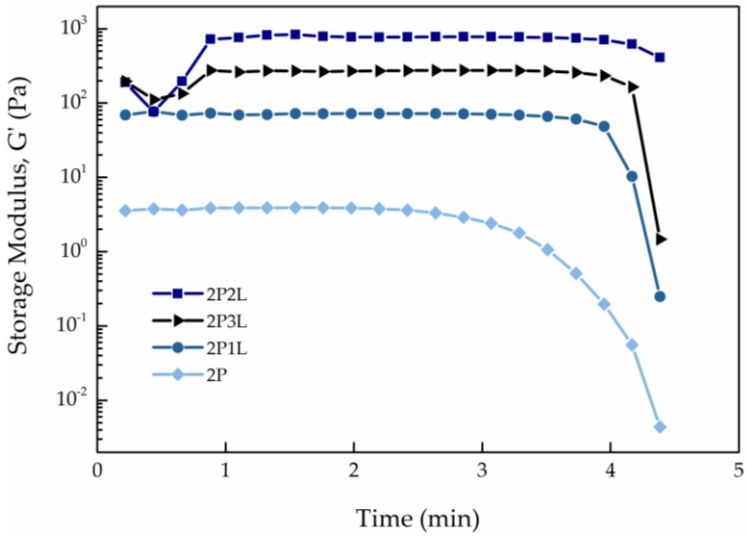

Figure 3.18 – Storage Modulus (*G'*) in function of time for all compositions.

Regarding *G''*, displayed in Figure 3.19, the obtained curves followed the same trend as *G'*, with laponite groups showing higher modulus. This modulus refers to the internal friction between

molecules and particles of the studied fluid, from which energy is dissipated when this deformation is turned into heat. Therefore, it is comprehensible that the more viscous a fluid is, the more friction will exist between its microstructure constituents.

However, both 2P2L and 2P3L showed some unexpected peaks in the constant region. This might indicate some temporary disturbances in their microstructures. However, no explanation was found in the literature for such an event nor this analysis could be continued in order to explain such behavior.

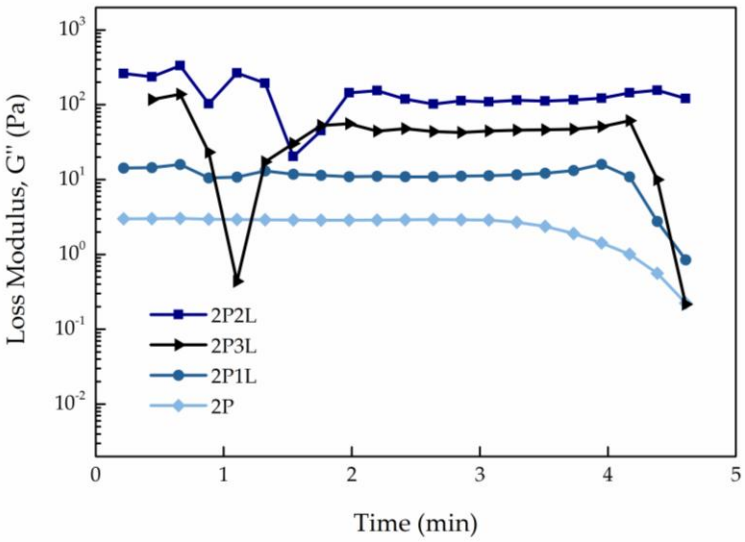

Figure 3.19 - Loss Modulus (G'') in function of time for all compositions.

By intersecting *G'* and *G''* plots (Figure 3.20), it is possible to determine the flow point, i.e., the point from which the fluid switches from solid-like to liquid-like behavior. The point where both moduli intersect corresponds to the start of the printing process in an extrusion-based system. The intersection between both moduli for the 4 studied compositions can be found Figure 3.20. 2P showed a flow point at a lower shear load, as expected, while 2P1L and 2P3L both started to flow after the 4th minute, almost at the maximum shear stress. Unfortunately, the rheology results were obtained in function of time, making it impossible to define the exact shear load at which the flowing point occurred.

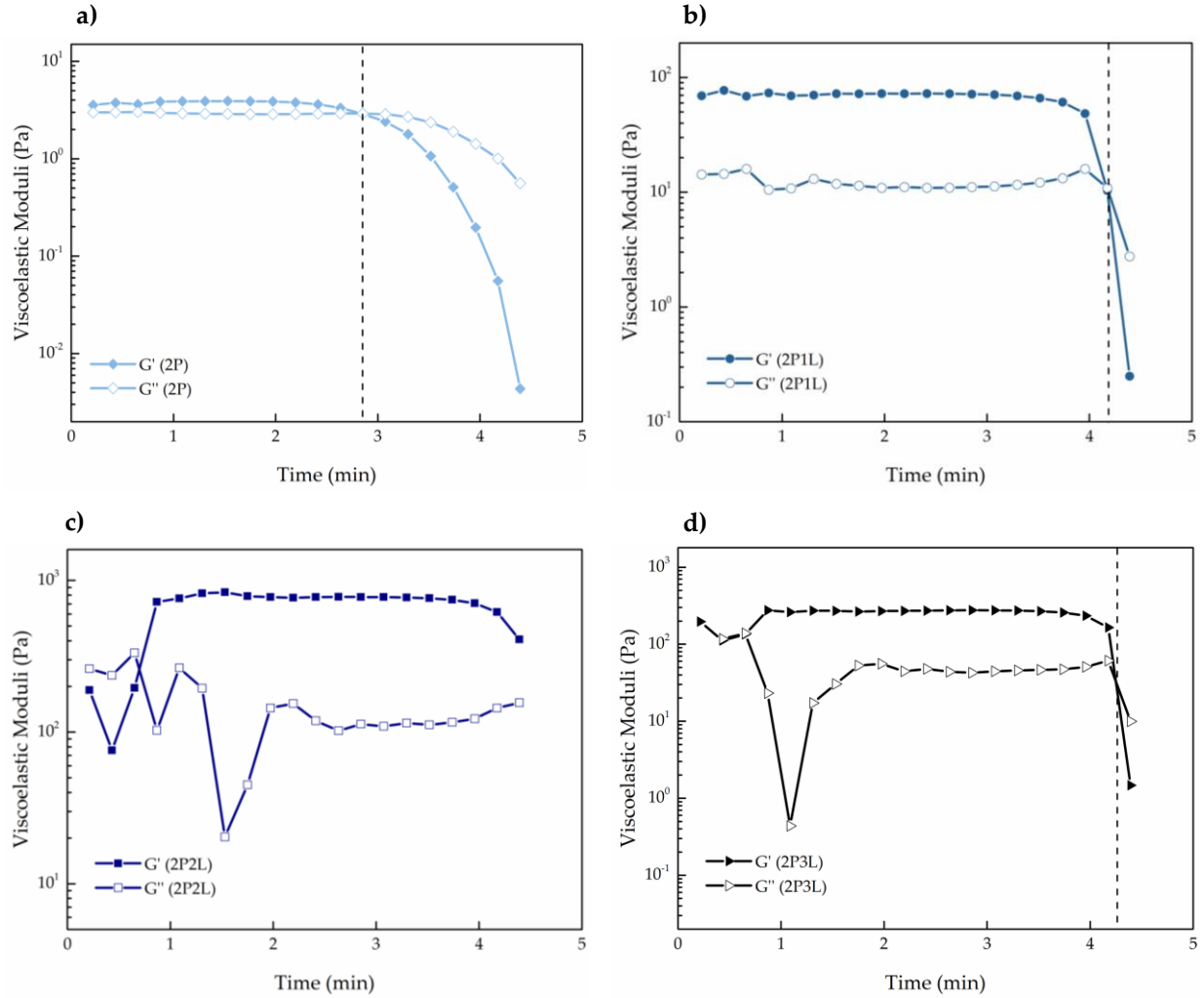

Figure 3.20 – Intersection of *G'* and *G''* plot lines for a) 2P, b) 2P1L, c) 2P2L and d) 2P3L in order to observe the flow point.

3.6. 3D Printing and Printability Quantification

In this section, a printability window for PEMA and PEMA/LAP hydrogels was determined and the printable compositions were parametrically quantified. Firstly, the jets of the 4 suggested inks were analyzed, followed by quantification of square grid and stacked constructs of the printable compositions.

In Figure 3.21 one can find the printing jets of the 4 compositions. Starting from the right, the first picture belongs to 2P (a)), followed by 2P1L, 2P2L and 2P3L (b), c) and d), respectively). Jet transformation along the different compositions with the increase of laponite is clearly visible. 2P jet exhibited a typical behavior of liquid inks, forming a droplet after exiting the nozzle. Figure 3.21 e) shows the printing of PEMA 2% onto a glassing slide, where an expansion after extrusion is visible due to the droplet-like jet. F. Munarin *et al.* [22] managed to print this same composition by applying a pre-crosslinking step in order to increase its viscosity, as previously reported in the introduction section.

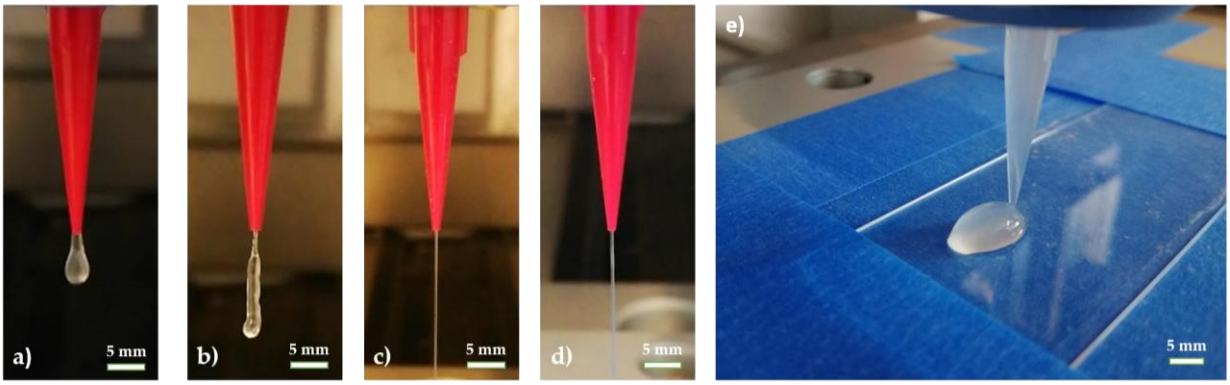

Figure 3.21 - a), b), c) and d) Jet pictures of 2P, 2P1L, 2P2L and 2P3L, respectively, at a pressure of 0.08 MPa; d) Picture of 2P's expansion after printing.

The incorporation of LAP 1 wt.% proved to have an impact on the hydrogel's viscosity, as proved by the previously shown rheology study, which consequently impacted the extrusion jet. Despite 2P1L viscosity still not being in the required range for extrusion-based 3D printing, the addition of the nanosilicate was enough to eliminate the droplet-like jet. However, as one can see in Figure 3.21 b), the jet still exhibits inconsistencies and expands after exiting the nozzle. Finally, the shear-thinning behavior of laponite allowed 2P2L and 2P3L viscous inks to have a continuous and consistent jet, making these two the printable compositions among the ones which were studied in this work.

PEMA 1 wt.% doesn't provide the necessary ink viscosity, not even with the incorporation of laponite. Higher concentrations of laponite, starting at 4 wt.%, not only make the inks too much viscous but also difficult blending between LAP and PEMA solutions. Having this in consideration and from the analysis of the jets, it was possible to define a printability window (adapted from [43]), that can be found in Figure 3.22.

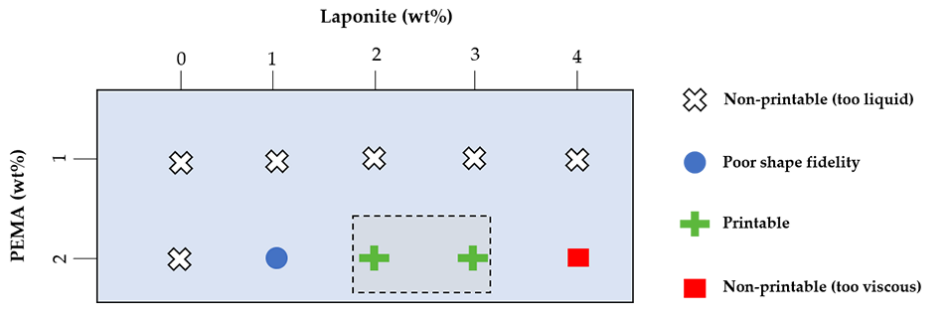

Figure 3.22 - Printability window diagram.

In order to quantify 2P3L and 2P2L printability, these were printed with different shapes and stacking heights. Square grids with 1, 2, and 3 mm inner squares were printed for both compositions, and can be found in Figure 3.23, whereas hollow squares with 5, 10 and 20 layers in height are displayed in Figure 3.24, that was only placed further in this section since it was only used for height fidelity, which will be the last parameter to be discussed.

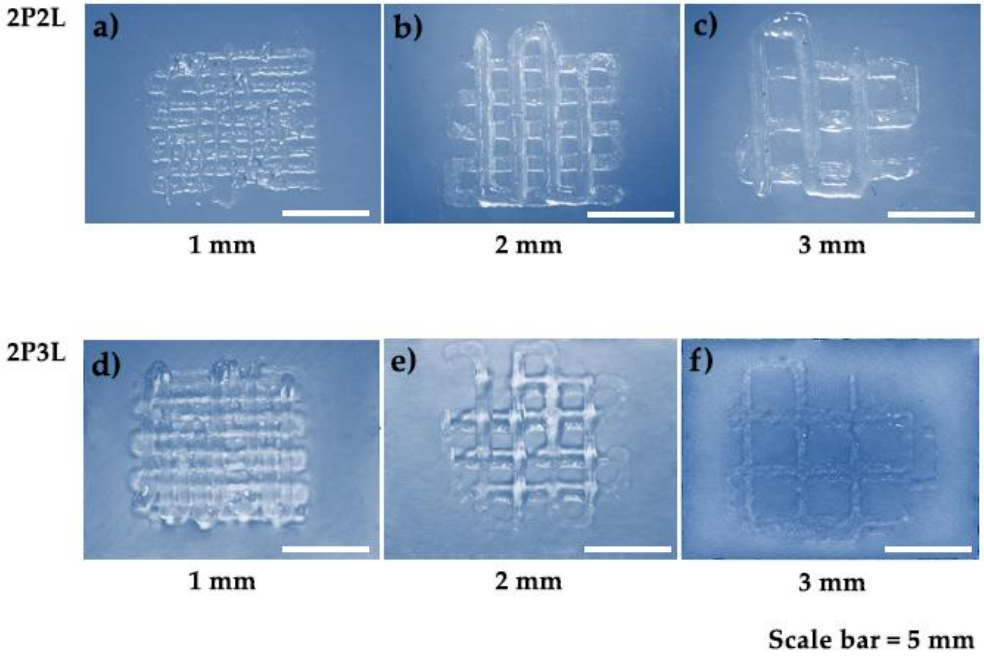

Figure 3.23 – Stereoscope pictures of square grid printed constructs 1, 2, and 3 mm square size for 2P2L (a-c) and 2P3L (d-f).

The square grid shapes, exhibited above, were used to quantify 3 parameters: printability ratio, spreading ratio and shape fidelity.

3.6.1. Printability Ratio

The printability ratio was adapted from [44], where it was used to quantify the printing of cell-laden gelatin/alginic acid sodium salt bioinks. This parameter analyzes the squareness of the printed square shape, i.e., how similar the printed squares are, in terms of geometry, compared to the pre-designed ones. The more squared the printed square is, the closer PR is to 1. If the square exhibits a rounded shape, $PR<1$, whereas odd shapes have a $PR>1$. This parameter can be calculated by using equation (3.3), that relates the square's area (A) and perimeter (L):

$$Printability\ Ratio\ (PR) = \frac{L^2}{16A} \quad (3.3)$$

In this work, as in [44], a PR acceptance window of 0.8 < PR < 1.1 was established. Statistical analysis was not performed for this parameter since the values were so close to one another. 6 squares from each square grid were measured.

As one can see in Table 3.1, most of the values fell within the acceptance window. Starting with 2P2L, the biggest value was exhibited by the smallest square grid (1 mm), with a PR of 1.10 ± 0.08, just in the limits of the established window. Both 2 and 3 mm showed values closer to 1 (0.99 ± 0.03 and 1.02 ± 0.03, respectively). 2P3L showed a PR of 1.12 for both 1 and 2 mm square grids, with SD of 0.07 and 0.05, respectively. 2P3L's wider grid (3 mm) exhibited a PR of 0.99 ± 0.02. So, every square grid except for the 1 and 2 mm ones belonging to 2P3L fell between 0.8 and 1.1.

Comparing the square grids with the same square size, only 2 mm showed significantly different PRs (0.99 ± 0.03 for 2P2L against 1.12 ± 0.05 for 2P3L), with 2P3L staying out of the acceptance window. 3 mm printed grids showed very similar values, both inside the 0.8 – 1.1 range. Lastly, 1 mm square grids also exhibited similar PRs, even though one can consider that the grid corresponding to 2P3L stayed out of the desired PR range.

Table 3.1 - Printability Ratio of 1, 2 and 3 mm printed square grids for 2P2L and 2P3L.

Printability Ratio	**1mm**	**2mm**	**3mm**
2P2L	1.10 ± 0.08	0.99 ± 0.03	1.02 ± 0.03
2P3L	1.12 ± 0.07	1.12 ± 0.05	0.99 ± 0.02

3.6.2. Spreading Ratio

The spreading ratio can be defined as the ratio between the width of the printed filament and the internal diameter of the used nozzle, as stated in equation (3.4):

$$Spreading\ Ratio\ (SPR) = \frac{Printed\ fillament\ width}{Nozzle\ internal\ diameter} \quad (3.4)$$

This parameter was adapted from [45], where it was used to quantify the printability of alginate bioinks with different molecular weights and crosslinking ratios. In this work, a 25 G conical nozzle was used with an internal diameter of 0.25 mm. In order to quantify the square grids displayed in Figure 3.23, the line width was measured in 10 different locations along each grid.

Table 3.2 presents the SR for all compositions and correspondent square grids. Statistical analysis was used to compare the spreading ratio values between the two compositions. The significance proportionally increased with the square size: * for 1 mm squares (p_v=0.0179), ** for 2 mm (p_v=0.0015) and *** for 3 mm (p_v=0.0004).

For 1 mm square grids, the increase of laponite caused the SR to rise from 1.5 ± 0.1 to 2.1 ± 0.3. On the other hand, both 2 and 3 mm square grids showed an opposite behavior, with SR decreasing from 3.2 ± 0.2 to 2.4 ± 0.4 for 2 mm and from 3.2 ± 0.3 to 2.3 ± 0.4 for 3 mm. One can also notice that for 2P2L the increasing of the square size resulted in SR increasing, as expected, since the smaller the square size is the closer the filaments are, resulting in limited expansion/spreading.

Table 3.2 - Spreading Ratio of 1, 2 and 3 mm printed square grids for 2P2L and 2P3L.

Spreading Ratio	**1 mm**	**2 mm**	**3 mm**
2P2L	1.5 ± 0.1	3.2 ± 0.2	3.2 ± 0.3
2P3L	2.1 ± 0.3	2.4 ± 0.4	2.3 ± 0.4

3.6.3. Shape Fidelity

G. Han *et al*. [46] reported a shape fidelity parameter to quantify the printing of decellularized ECM-based 3D cell-laden constructs. This parameter compares the theoretical area of a square (A_{te}) with the real one obtained for the printed construct (A_{re}), as demonstrated by equation (3.5):

$$Shape\ Fidelity\ (SF)(\%) = \frac{A_{re}}{A_{te}} \times 100 \quad (3.5)$$

6 squares from each square grid were measured in order to quantify this parameter. As it happened for SR, statistical analysis was used to examine the significance between 2P2L and 2P3L for the correspondent square grids. For the largest grid (3 mm) the differences were considered to be not-significant, which can be easily understandable by looking at the SF values (35.4 ± 2.1 for 2P2L and 38.2 ± 1.7). This analysis also showed a significant difference of ** for 1 mm square grids (p_v=0.0039) and a * one for the 2 mm grids (p_v=0.0138).

Regarding 1 mm square grids, the increasing of laponite resulted in the decreasing of shape fidelity from 17.0 ± 2.4 % to 7.3 ± 1.1 %. Even though they were printed using the same CAD-file, by looking at Figure 3.23 a) and d) it is noticeable that the square grids are distinct, and that some of the filaments end up merging with each other after printing, obstructing the squares. This is in accordance with the spreading ratio analysis, which showed a higher spreading for 2P3L. The same relation between SF and SPR can be applied for 2 mm grids. SF decreased from 22.8 ± 1.8 % for 2P3L to 14.3 ± 2.3 % for 2P2L, following the same trend as spreading ratio, where 2P2L exhibited a higher value (see Table 3.2).

Table 3.3 – Shape fidelity of 1, 2 and 3 mm printed square grids for 2P2L and 2P3L.

Shape Fidelity (%)	**1 mm**	**2 mm**	**3 mm**
2P2L	17.0 ± 2.4	14.3 ± 2.3	35.4 ± 2.1
2P3L	7.3 ± 1.1	22.8 ± 1.8	38.2 ± 1.7

3.6.4. Height Fidelity

To complete printability quantification, the height fidelity of stacked constructs was analyzed. This parameter was adapted from the previous discussed parameter (SF), as it is also a comparison between a theoretical and a real value. 2P2L and 2P3L constructs were printed with 5, 10 and 20 layers, and their real height (H_{re}), was compared to the theoretical one (H_{te}), as stated in equation (3.6):

$$Height\ Fidelity\ (HF)(\%) = \frac{H_{re}}{H_{te}} \times 100 \quad (3.6)$$

Stereoscope pictures of the different stacking layers for each composition can be found in Figure 3.24.

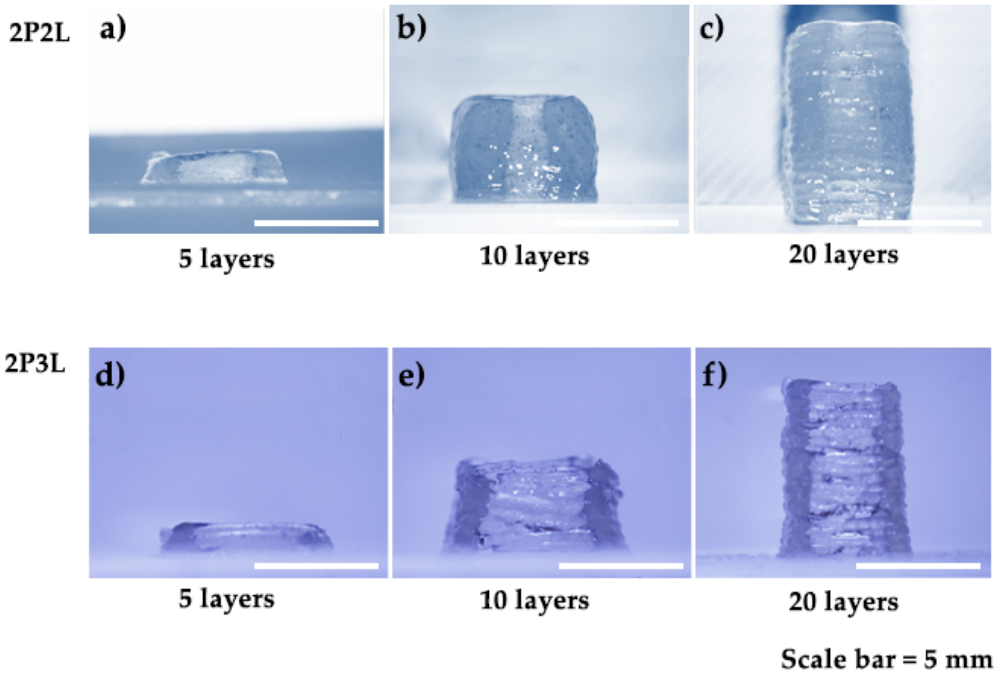

Figure 3.24 – Steoreoscope pictures of stacked constructs with 5, 10 and 20 layers. a,b,c) Stacked constructs for 2P2L; d,e,f) Stacked constructs for 2P3L.

Constructs' height was measured in 3 different zones. The averages of these measurements and correspondent SDs can be found in Table 3.4. The statistical analysis stated that the differences between 2P2L and 2P3L, considering the same number of layers, were not significant. However, rather than analyze the differences in HF for the same stackings, one can analyze the impact of layer increasing on HF. Regarding 2P2L, it is clear that the increase on number of layers had a positive impact on height fidelity, which went from 72.5 ± 5.5 % for 5 layers to 96.6 ± 1.8 % for 20 layers. The same trend was followed by 2P3L, which exhibited a 68.3 ± 5.4 % height fidelity for the lower stacking and a remarkable 97.4 ± 1.1 % for the higher one. This can be explained by looking at Figure 3.24 a) and d), where it is visible that the top of the 5 layers constructs is not as horizontally straight as it is for 10 and 20 layer stackings, showing variable heights along the construct's length.

Table 3.4 - Height Fidelity for 5, 10 and 20 layers stacked constructs for 2P2L and 2P3L.

Height Fidelity (%)	**5 layers**	**10 layers**	**20 layers**
2P2L	72.5 ± 5.5	93.8 ± 1.8	96.6 ± 1.8
2P3L	68.3 ± 5.4	86.9 ± 1.1	97.4 ± 1.1

4. Conclusions and Future Perspectives

This project was developed in the Orthopaedics Department of University Medical Centre Utrecht, in collaboration with the Department of Health Technology of the Technical University of Denmark. The aim of it was to develop 3D-printable laponite reinforced pectin-methacrylate hydrogels as alternatives for bone tissue engineering. Therefore, laponite concentration was studied and optimized by performing a wide range of characterization techniques.

Firstly, FTIR analysis was used to confirm the UV-crosslinking of the hydrogel system. The shift of the peak corresponding to Amide I and the extinction of the =CH peak of the acrylate groups after crosslinking confirmed that the photopolymerization was indeed achieved after 10 minutes of UV-exposure. Swelling ratio and degradation can also be used as proof that crosslinking was in fact achieved since the hydrogel discs would not be able to remain stable over a period of 21 days if they were not crosslinked. Laponite incorporation proved to highly impact these two domains, especially hydrogel swelling, with a remarkable 26% decrease being registered when comparing PEMA 2 wt.%: Laponite 3 wt.% with PEMA 2 wt.%. Swelling ratio decreased linearly with laponite concentration. Despite not so evident, a similar impact was reported for degradation rate, with all the groups showing a degradation of less than 40%, which is remarkable.

As for morphological characterization, the porosity of freeze-dried discs of the 4 compositions was analyzed through SEM observation of vertical cross-sections of the scaffolds. The reinforcement of PEMA's network proved to have an effect on the scaffolds' pore size. Average pore size went from 196 ± 103 μm for the merely polymeric discs to 78 ± 22 μm for the discs reinforced with 3 wt.% laponite. However, 2P1L and 2P2L exhibited average pore sizes above 100 μm, which is defined as the minimum recommended pore size for effective bone regeneration. Laponite incorporation also showed to decrease the variety of pore sizes. However, the decrease was not in such an order that poses a threat to the flow of substances in and out of the scaffold.

Compressive tests were used to obtain elastic modulus, toughness and compressive strength of the studied groups, while cyclic tests were also performed in order to assess the energy loss after the 1st cycle and the decrease in strength after 5 cycles. Regarding the compressive tests, the group which generally showed the best results was 2P2L. Toughness and compressive strength were higher for this group, showing increases around a 4-fold order when compared to 2P. Despite this, 2P3L exhibited the higher elastic modulus, registering an impressive 40 kPa increase when compared to PEMA 2 wt.%. The elastic modulus of 48.1 ± 0.7 kPa perfectly fell within the 25 – 65 kPa range of optimal values for osteogenesis, as suggested by [13]. Regarding cyclic tests, laponite increasing was associated with a higher decrease in strength after 5 cycles, which might be explained by the higher brittleness of the scaffolds due to the incorporation of the nanosilicate. Also, these groups exhibited a higher energy loss after 1 cycle, proving that laponite nanoplatelets absorb some of the load energy while compressed.

Prior to 3D printing, a rheology study was carried out to quantify the viscosities of the hydrogels and to observe the shear-thinning behavior of laponite groups. Laponite groups exhibited higher viscosities and their shear-thinning behavior was also clear, with viscosities dramatically decreasing when a shear rate was applied. This decrease was proportional with the increase of laponite wt.%, as expected. G' and G'' also increased proportionally with laponite until 2 wt.%. LVE region was longer for LAP groups, with the flow point occurring at higher shear rates than for PEMA 2 wt.%.

Studies progressed towards the final step of this study, which was to define a printability window and to quantify the printable compositions. 2P2L and 2P3L exhibited continuous extrusion jets and were considered to be the 2 printable compositions among the studied ones. Both compositions exhibited satisfying results for the analyzed printability parameters regarding shape fidelity, printability ratio, and spreading ratio, especially for 2 and 3 mm square grids. Height fidelity of stacked constructs was also analyzed, with 20-layer stackings exhibiting the highest value, reporting fidelities around 97% for both inks, which is astonishing.

One can say that laponite incorporation into PEMA hydrogels had an outstanding impact on scaffolds' properties. Overall, PEMA 2 wt.%: Laponite 2 wt.% exhibited the most promising properties, surpassing PEMA 2 wt.%: Laponite 3 wt.%. 2P3L was associated with either stagnation or even a decrease in the hydrogels' properties when compared to 2P2L. These results imply the existence of a saturation limit for laponite's concentration, from which scaffolds' properties are no longer boosted by nanosilicate incorporation. Such behavior can be explained by laponite nanoplatelets agglomeration, which leads to a weaker interaction between laponite and PEMA's network. Such findings were also reported by [28] and [47].

In order to use these scaffolds in the clinic, several steps still need to be taken. Future works on this matter can be focused on:

1) Bioactivity study in order to confirm that laponite association with pectin-methacrylate enhances osteogenic properties. This study was started during this thesis but unfortunately it could not be finished;
2) Optimization of printing parameters such as speed rate, pressure and nozzle distance in order to achieve better printability results. Several shapes should also be tested to quantify printability in that domain;
3) Cell-culture studies in order to define the best laponite concentration, for example Live/Dead assays or some tests with early-bone markers, like Alkaline Phosphatase;
4) Seeding cells into the hydrogels and study cell viability post-printing;
5) The addition of a biological component to this nanocomposite might be needed to increase its biological performance. It must be noted that in this project some approaches were tried, including the addition of gelatin-methacrylate, bone ECM particles and fibronectin to the hydrogel system. However, these strategies were abandoned especially due to incompatibilities regarding 3D printing. Further studies in this direction must have this into consideration;
6) After all the previous steps, the scaffolds still need to be tested in an *in vivo* environment.

5. References

[1] G. Hannink and J. J. C. Arts, “Bioresorbability, porosity and mechanical strength of bone substitutes: What is optimal for bone regeneration?,” *Injury*, vol. 42, no. SUPPL. 2, pp. S22–S25, 2011.

[2] S. Bose, M. Roy, and A. Bandyopadhyay, “Recent advances in bone tissue engineering scaffolds,” *Trends Biotechnol.*, vol. 30, no. 10, pp. 546–554, 2012.

[3] Holback, H. & Yeo, Yoon & Park, K.. (2011). "Hydrogel swelling behavior and its biomedical applications". 10.1533/9780857091383.1.3.

[4] Zhang, Yu & Khademhosseini, Ali. (2017). "Advances in engineering hydrogels". Science. 356. eaaf3627. 10.1126/science.aaf3627.

[5] E. Caló and V. V Khutoryanskiy, “Biomedical applications of hydrogels : A review of patents and commercial products,” vol. 65, pp. 252–267, 2015.

[6] S. Utech and A. R. Boccaccini, "A review of hydrogel-based composites for biomedical applications: enhancement of hydrogel properties by addition of rigid inorganic fillers", vol. 51, no. 1. Springer US, 2016.

[7] J. L. Drury and D. J. Mooney, “Hydrogels for tissue engineering : scaffold design variables and applications,” vol. 24, pp. 4337–4351, 2003.

[8] Afewerki, Samson & Sheikhi, Amir & Kannan, Soundarapandian & Ahadian, Samad & Khademhosseini, Ali. (2018). "Gelatin-Polysaccharide Composite Scaffolds for 3D Cell Culture and Tissue Engineering: Towards Natural Therapeutics". Bioengineering & Translational Medicine. 4. 10.1002/btm2.10124.

[9] Silva, Amanda & Juenet, Maya & Pelle, Anne & Letourneur, Didier. (2015). "Polysaccharide-based strategies for heart tissue engineering". Carbohydrate polymers. 116. 267-77. 10.1016/j.carbpol.2014.06.010.

[10] M. A. Barbosa, P. L. Granja, C. C. Barrias, and I. F. Amaral, “Polysaccharides as scaffolds for bone regeneration,” *Itbm-Rbm*, vol. 26, no. 3, pp. 212–217, 2005.

[11] Radhakrishnan, Janani & Subramanian, Anuradha & Krishnan, Uma & Sethuraman, Swaminathan. (2016). "Injectable and 3D Bioprinted Polysaccharide Hydrogels: From Cartilage to Osteochondral Tissue Engineering". Biomacromolecules. 18. 10.1021/acs.biomac.6b01619

[12] T. M. Aminabhavi, “Polysaccharide-Based Hydrogels as Biomaterials in Drug Delivery,” *J. Pharm. Care Heal. Syst.*, vol. 02, no. 03, pp. 10–11, 2015.

[13] Mehrali, Mehdi & Thakur, Ashish & Kadumudi, Firoz & Pierchala, Malgorzata & Vacacela Cordova, Julio & Shahbazi, Mohammad-Ali & Mehrali, Mohammad & Pennisi, Cristian & Orive, Gorka & Gaharwar, Akhilesh & Dolatshahi-Pirouz, Alireza. (2019). "Pectin Methacrylate (PEMA) and Gelatin-Based Hydrogels for Cell-Delivery: Converting Waste-Materials into Biomaterials". ACS Applied Materials & Interfaces. 11. 10.1021/acsami.9b00154.

[14] B. R. Thakur *et al.*, “Chemistry and uses of pectin — A review Chemistry and Uses of Pectin — A Review,” vol. 8398, no. December, 2017.

[15] T. Katav, L. Liu, T. Traitel, R. Goldbart, M. Wolfson, and J. Kost, “Modified pectin-based carrier for gene delivery : Cellular barriers in gene delivery course,” *J. Control. Release*, vol. 130, no. 2, pp. 183–191, 2008.

[16] Z. Hussain, H. Katas, S. L. Yan, and D. Jamaludin, “Efficient Colonic Delivery of DsiRNA by Pectin-Coated Polyelectrolyte Complex Nanoparticles: Preparation, Characterization and Improved Gastric Survivability,” pp. 1016–1027, 2018.

[17] Liu, Lucian & Fishman, Marshall & Hicks, Kevin. (2007). "Pectin in controlled drug delivery - A review". Cellulose. 14. 15-24. 10.1007/s10570-006-9095-7.

[18] T. W. Wong, G. Colombo, and F. Sonvico, “Pectin Matrix as Oral Drug Delivery Vehicle for Colon Cancer Treatment”, vol. 12, no. 1, 2011.

[19] W. Zhang, P. Xu, and H. Zhang, "Pectin in Cancer Therapy: A Review", *Trends Food Sci. Technol.*, 2015.

[20] Munarin, Fabiola & Guerreiro, Susana & Grellier, M.A. & Tanzi, Maria & Barbosa, Mário & Petrini, Paola & Granja, Pedro. (2011). "Pectin-Based Injectable Biomaterials for Bone Tissue Engineering. Biomacromolecules". 12. 568-77. 10.1021/bm101110x.

[21] I. Industriale, "Panotan Exopolysaccharide - Based Hydrogel for Skeletal Muscle Tissue Engineering Application," 2018.

[22] Pereira, Rúben & Sousa, Aureliana & Barrias, Cristina & Bártolo, Paulo & Granja, Pedro. (2018). "A single-component hydrogel bioink for bioprinting of bioengineered 3D constructs for dermal tissue engineering". Materials Horizons. 10.1039/C8MH00525G.

[23] M. K. Jaiswal *et al.*, "Bioactive Nanoengineered Hydrogels for Bone Tissue Engineering: A Growth-Factor-Free Approach," *ACS Nano*, vol. 9, no. 3, pp. 3109–3118, 2015.

[24] L. Tao, L. Zhonglong, X. Ming, Y. Zezheng, L. Zhiyuan, and Z. Xiaojun, "RSC Advances carboxymethyl chitosan / LAPONITE ® composite," *RSC Adv.*, vol. 7, pp. 54100–54110, 2017.

[25] M. Mehrali, A. Thakur, C. P. Pennisi, and S. Talebian, "Nanoreinforced Hydrogels for Tissue Engineering : Biomaterials that are Compatible with Load-Bearing and Electroactive Tissues," 2017.

[26] J. M. Fraile *et al.*, European Journal of Pharmaceutics and Biopharmaceutics "Laponite as carrier for controlled in vitro delivery of dexamethasone in vitreous humor models", vol. 108, pp. 83–90, 2016.

[27] T. B. Becher, M. C. P. Mendonça, M. A. De Farias, M. B. De Jesus, and C. Ornelas, "Biological and Medical Applications of Materials and Interfaces Soft Nanohydrogels Based On Laponite Nanodiscs : A Versatile Drug Delivery Platform For Theranostics And Drug Cocktails Soft Nanohydrogels Based On Laponite Nanodiscs : A Versatile Drug Deliv," 2018.

[28] N. Golafshan, R. Rezahasani, M. Tarkesh Esfahani, M. Kharaziha, and S. N. Khorasani, "Nanohybrid hydrogels of laponite: PVA-Alginate as a potential wound healing material", vol. 176. Elsevier Ltd., 2017.

[29] U. E. D. E. Campinas, "Rheological studies and 3D extrusion-based printing of nanocomposite hydrogels Estudos reológicos e impressão 3D baseada em extrusão de hidrogéis nanocompósitos Rheological studies and 3D extrusion-based printing of nanocomposite hydrogels Estudos reológi," 2018.

[30] C. Ley, J. Brendlé, A. Walter, P. Jacques, A. Ibrahim, and X. Allonas, "On the interaction of triarylmethane dye crystal violet with LAPONITE® clay: using mineral nanoparticles to control the dye photophysics," *Phys. Chem. Chem. Phys.*, vol. 17, no. 26, pp. 16677–16681, 2015.

[31] M. Shahbazi *et al.*, "Combinatorial Screening of Nanoclay-Reinforced Hydrogels: A Glimpse of the ' Holy Grail ' in Orthopedic Stem Cell Therapy?," 2018.

[32] Ahlfeld, Tilman & Cidonio, Gianluca & Kilian, David & Duin, Sarah & Akkineni, Ashwini Rahul & Dawson, Jonathan & Yang, Shoufeng & Lode, Anja & Oreffo, Richard & Gelinsky, Michael. (2017). "Development of a clay based bioink for 3D cell printing for skeletal application. Biofabrication". 9. 10.1088/1758-5090/aa7e96.

[33] Ashammakhi, Nureddin & Hasan, MD Anwarul & Kaarela, Outi & Byambaa, Batzaya & Sheikhi, Amir & Gaharwar, Akhilesh & Khademhosseini, Ali. (2019). "Advancing Frontiers in Bone Bioprinting". Advanced Healthcare Materials. 8. 1801048. 10.1002/adhm.201801048.

[34] Panwar, Amit & Tan, Lay Poh. (2016). "Current Status of Bioinks for Micro-Extrusion-Based 3D Bioprinting. Molecules". 21. 685. 10.3390/molecules21060685.

[35] Mannoor, Manu & Jiang, Ziwen & James, Teena & Kong, Yong & Malatesta, Karen & Soboyejo, W. & Verma, Naveen & Gracias, David & McAlpine, Michael. (2013). "3D Printed Bionic Ears". Nano letters. 13. 10.1021/nl4007744.

[36] Hockaday, Laura & Kang, Kevin & Colangelo, Nicholas & Cheung, P & Duan, Bin & Malone, E & Wu, Jun & Girardi, L & Bonassar, Lawrence & Lipson, H & Chu, Cc & Butcher, Jonathan. (2012). "Rapid 3D printing of anatomically accurate and mechanically heterogeneous aortic valve

hydrogel scaffolds". Biofabrication. 4. 035005. 10.1088/1758-5082/4/3/035005.

[37] Mandrycky, Christian & Wang, Daniel Zongjie & Kim, Keekyoung & Kim, Deok-Ho. (2015). "3D Bioprinting for Engineering Complex Tissues". Biotechnology Advances. 34. 10.1016/j.biotechadv.2015.12.011.

[38] P. Schmidt, J. Dybal, and M. Trchova, "Investigations of the hydrophobic and hydrophilic interactions in polymer – water systems by ATR FTIR and Raman spectroscopy," vol. 42, pp. 278–283, 2006.

[39] G. David and S. S. Maier, "Micro- / Nanostructured polymeric materials : Poly (ε -caprolactone) crosslinked collagen sponges," no. January 2015, 2020.

[40] Mahdavinia, Gholam & Ettehadi, Sanaz & Amini, Mojtaba & Sabzi, Mohammad. (2015). "Synthesis and characterization of hydroxypropyl methylcellulose-g-poly(acrylamide)/LAPONITE® RD nanocomposites as novel magnetic- and pHsensitive carriers for controlled drug release". RSC Advances. 5. 44516-44523. 10.1039/C5RA03731J.

[41] H. Pálková, J. Madejová, M. Zimowska, and E. M. Serwicka, "Microporous and Mesoporous Materials Laponite-derived porous clay heterostructures : II . FTIR study of the structure evolution," *Microporous Mesoporous Mater.*, vol. 127, no. 3, pp. 237–244, 2010.

[42] Ganji, Fariba & Vasheghani Farahani, Samira & Vasheghani-Farahani, Ebrahim. (2010). "Theoretical Description of Hydrogel Swelling: A Review". Iranian Polymer Journal. 19. 375-398.

[43] P. Z. Id *et al.*, "Layer-by-layer ultraviolet assisted extrusion- based (UAE) bioprinting of hydrogel constructs with high aspect ratio for soft tissue engineering applications," pp. 1–21, 2019.

[44] M. Müller, J. Becher, and M. Schnabelrauch, "Effect of bioink properties on printability and cell viability for 3D bioplotting of embryonic stem cells," *Biofabrication*, vol. 8, no. 3, pp. 1–12.

[45] F. E. Freeman and D. J. Kelly, "Tuning Alginate Bioink Stiffness and Composition for Controlled Growth Factor Delivery and to Spatially Direct MSC Fate within Bioprinted Tissues," *Sci. Rep.*, no. November, pp. 1–12, 2017.

[46] G. Ahn *et al.*, "Precise stacking of decellularized extracellular matrix based 3D cell-laden constructs by a 3D cell printing system equipped with heating modules," *Sci. Rep.*, no. July, pp. 1–11, 2017.

[47] Du, Juan & Zhu, Jinlong & Wu, Ronglan & Xu, Shimei & Tan, Yun & wang, Jide. (2015). "A facile approach to prepare strong poly(acrylic acid)/LAPONITE® ionic nanocomposite hydrogels at high clay concentrations". RSC Adv.. 5. 10.1039/C5RA07651J.

6. Appendix

A. Laponite Microstructure

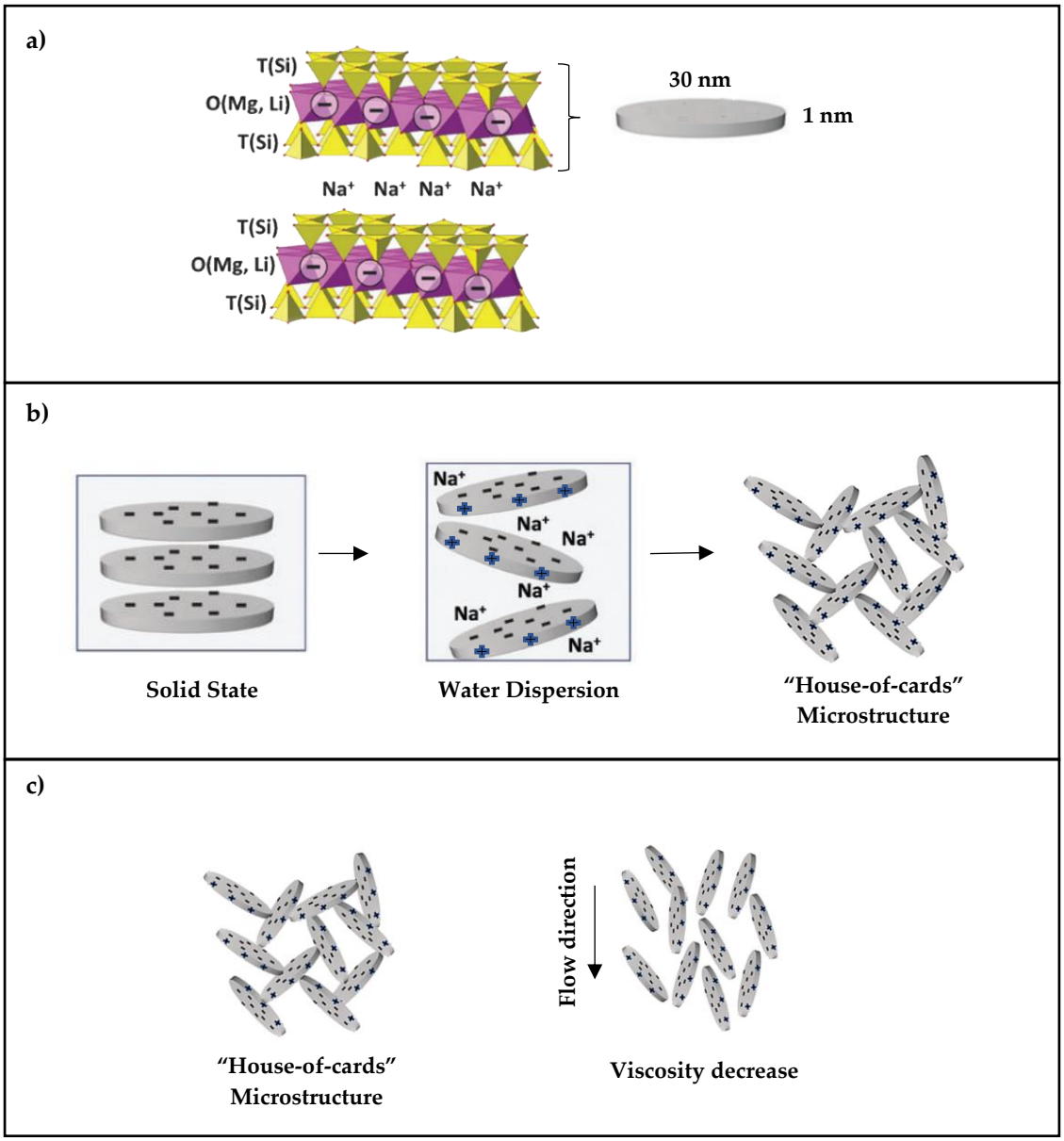

Figure 6.1 – Schematic of a) Laponite microstructure and its constituents, b) Laponite behavior when dispersed in water and c) shear-thinning behavior of the nanosilicate.

B. Pectin Methacrylation

Briefly, to prepare the medium-PEMA with 48.82% theoretical methacrylation of acidic carboxyl groups, the pectin powder (1 g) was mixed at 1% (w/v) into a 50 mM MES buffer solution (100 ml, pH 6.5) containing 0.5 M NaCl at room temperature. After the powder was completely dissolved, 0.69 g (60 mM) N-Hydroxysuccinimide (NHS) and 2.3 g (120 mM) 1-Ethyl-3-(3-dimethylaminopropyl)carbodiimide (EDC) were added to this solution and stirred for 10 min to activate the carboxylic acid groups of pectin. Afterward, 0.994 g (60 mM) AEMA was added to the solution and allowed to react for 24 hours at room temperature in the dark. The molar ratio of NHS:EDC:AEMA was maintained at 1:2:1. Low (30 mM) and high (90 mM) AEMA were used to synthesize low and high degree of PEMA methacrylation, while keeping the NHS:EDC:AEMA molar ratio constant. After 24 hours, the solution mixture was precipitated by the addition of excess acetone and dried under the fume hood. The resulting polymer was dehydrated and dissolved in 100 ml deionized water for further purification and subsequently dialyzed against DI water for 3 days and lyophilized.

C. Compression Setup

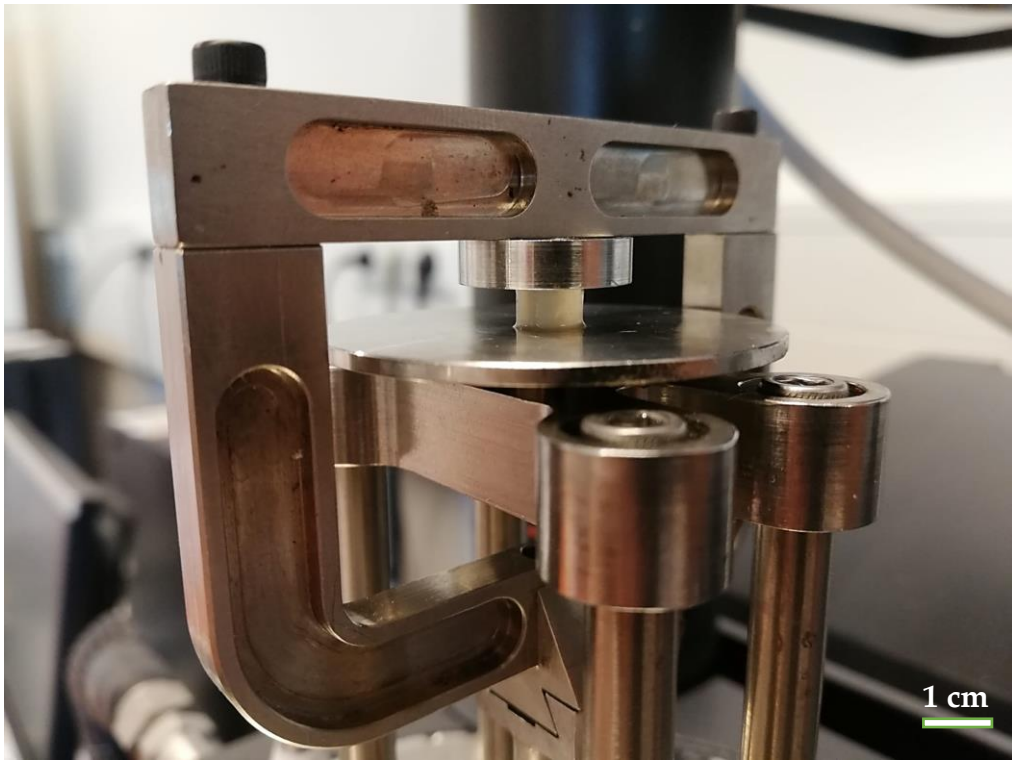

Figure 6.2 - Compression setup for both compression and cyclic tests.

D. Rheology Setup

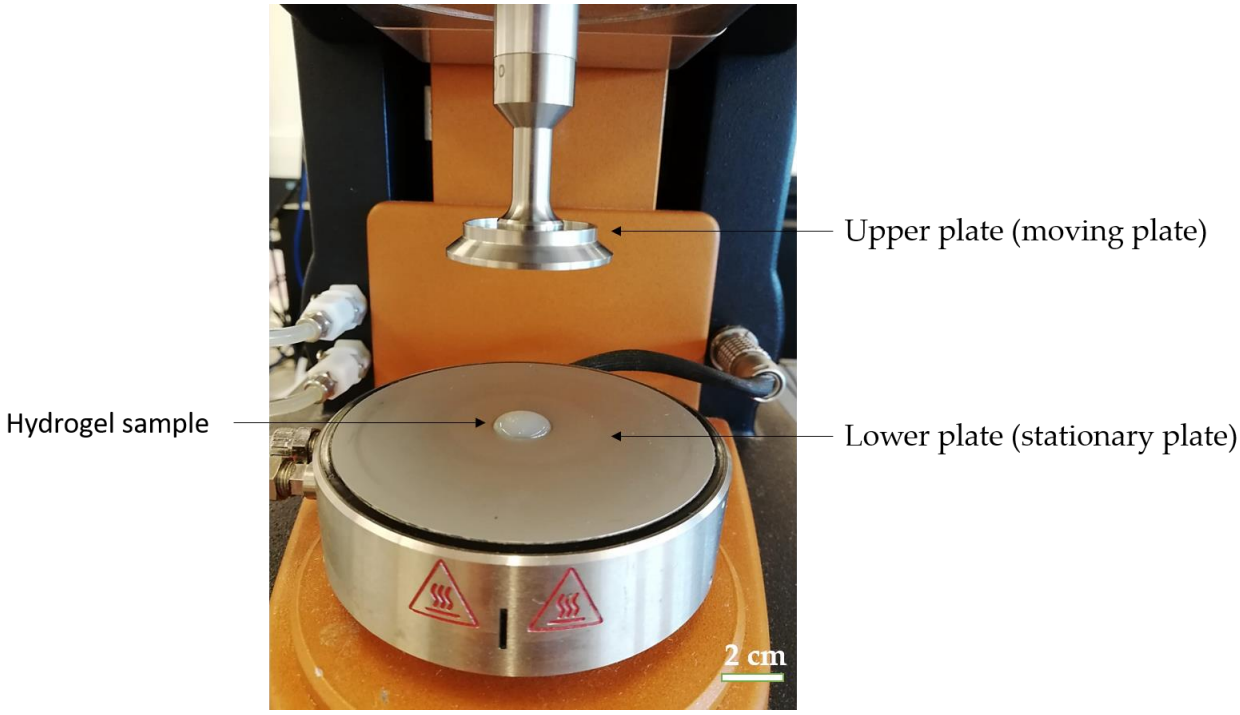

Figure 6.3 - Rheology setup for viscosity, G' and G'' assessment.

E. Statistical Analysis

Table 6.1 - Statistical analysis for swelling ratio, degradation rate, porosity, mechanical properties and printing parameters.

Technique	Compositions	p value	Summary	Significant
Swelling Ratio	2P vs 2P1L	0.0104	*	Yes
	2P vs 2P2L	0.0003	***	Yes
	2P vs 2P3L	<0.0001	****	Yes
	2P1L vs 2P2L	0.0576	ns	No
	2P1L vs 2P3L	0.0023	**	Yes
	2P2L vs 2P3L	0.1394	ns	No
Degradation Rate	2P vs 2P1L	0.8676	ns	No
	2P vs 2P2L	0.0103	*	Yes
	2P vs 2P3L	0.0004	***	Yes
	2P1L vs 2P2L	0.0040	**	Yes
	2P1L vs 2P3L	0.0002	***	Yes
	2P2L vs 2P3L	0.0646	ns	No
Porosity	2P vs 2P1L	0.3263	ns	No
	2P vs 2P2L	0.0143	*	Yes
	2P vs 2P3L	0.0007	***	Yes
	2P1L vs 2P2L	0.4772	ns	No
	2P1L vs 2P3L	0.0735	ns	No
	2P2L vs 2P3L	0.7188	ns	No
Elastic Modulus	2P vs 2P1L	0.0242	*	Yes
	2P vs 2P2L	<0.0001	****	Yes
	2P vs 2P3L	<0.0001	****	Yes
	2P1L vs 2P2L	<0.0001	****	Yes
	2P1L vs 2P3L	<0.0001	****	Yes
	2P2L vs 2P3L	0.7082	ns	No
Toughness	2P vs 2P1L	0.2249	ns	No
	2P vs 2P2L	0.0254	*	Yes

	2P vs 2P3L	0.0052	**	Yes
	2P1L vs 2P2L	0.5738	ns	No
	2P1L vs 2P3L	0.1728	ns	No
	2P2L vs 2P3L	0.8002	ns	No
Strength	2P vs 2P1L	0.0442	*	Yes
	2P vs 2P2L	0.0025	**	Yes
	2P vs 2P3L	0.0375	*	Yes
	2P1L vs 2P2L	0.3835	ns	No
	2P1L vs 2P3L	0.9997	ns	No
	2P2L vs 2P3L	0.4312	ns	No
Shape Fidelity	1 mm (2P2L vs 2P3L)	0.0039	**	Yes
	2 mm (2P2L vs 2P3L)	0.0138	*	Yes
	3 mm (2P2L vs 2P3L)	0.3533	ns	No
Height Fidelity	2P2L vs 2P3L (5 layers)	0.4805	ns	No
	2P2L vs 2P3L (10 layers)	0.0690	ns	No
	2P2L vs 2P3L (20 layers)	0.9992	ns	No
Spreading Ratio	1 mm (2P2L vs 2P3L)	0.0179	*	Yes
	2 mm (2P2L vs 2P3L)	0.0015	**	Yes
	3 mm (2P2L vs 2P3L)	0.0004	***	Yes

F. 1st Cycle Stress-Strain Curves

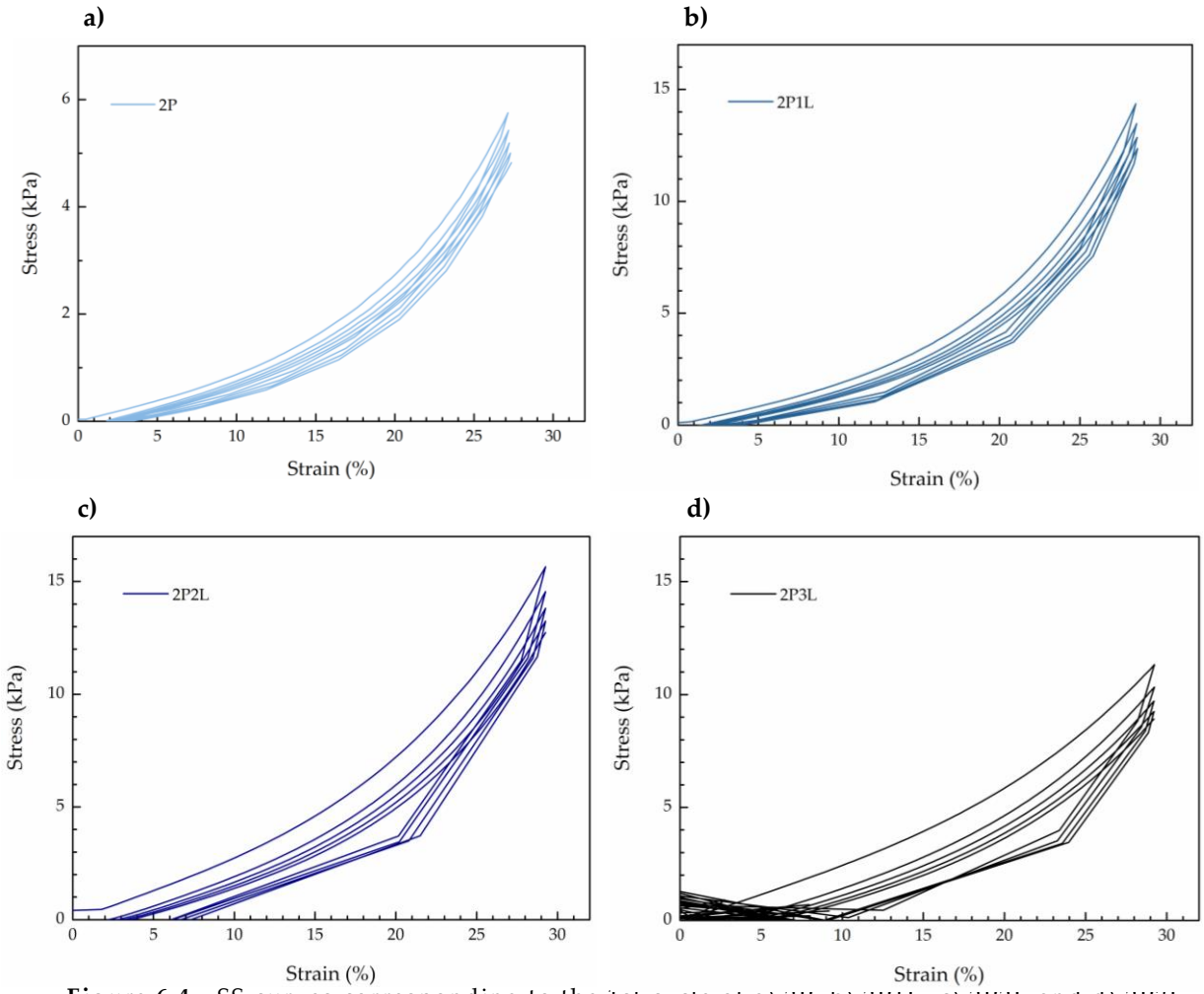

Figure 6.4 - SS curves corresponding to the 1st cycle of a) 2P, b) 2P1L, c) 2P2L and d) 2P3L.